

1 **A POSITIVE AND STABLE L2-MINIMIZATION BASED MOMENT**  
 2 **METHOD FOR THE BOLTZMANN EQUATION OF GAS DYNAMICS\***

3 NEERAJ SARNA<sup>†</sup>

4 **Abstract.** We consider the method-of-moments approach to solve the Boltzmann equation of  
 5 rarefied gas dynamics, which results in the following moment-closure problem. Given a set of mo-  
 6 ments, find the underlying probability density function. The moment-closure problem has infinitely  
 7 many solutions and requires an additional optimality criterion to single-out a unique solution. Mo-  
 8 tivated from a discontinuous Galerkin velocity discretization, we consider an optimality criterion  
 9 based upon L2-minimization. To ensure a positive solution to the moment-closure problem, we  
 10 enforce positivity constraints on L2-minimization. This results in a quadratic optimization prob-  
 11 lem with moments and positivity constraints. We show that a (Courant-Friedrichs-Lewy) CFL-type  
 12 condition ensures both the feasibility of the optimization problem and the L2-stability of the space-  
 13 time discrete moment approximation. We provide an extension of our method to multi-dimensional  
 14 space-velocity domains and perform several numerical experiments to showcase its accuracy.

15 **1 Introduction** Due to modeling assumptions, the Euler and the Navier-  
 16 Stokes equations become inaccurate as a flow deviates significantly from a thermo-  
 17 dynamic equilibrium. This motivates one to consider mathematical models that can  
 18 approximate flows in all regimes of thermodynamic non-equilibrium. One such model  
 19 is the Boltzmann equation (BE) that govern the evolution of a probability density  
 20 function (pdf)  $f(x, t, \xi) \in \mathbb{R}^+$  and reads

21 (1.1) 
$$\mathcal{L}(f) = 0 \quad \text{where} \quad \mathcal{L} := \partial_t + \xi \cdot \nabla - Q.$$

23 Above,  $\xi \in \mathbb{R}^{d_\xi}$  is the molecular velocity with  $1 \leq d_\xi \leq 3$  being the velocity-dimension,  
 24  $D := [0, T]$  is the temporal domain with  $T > 0$  being the final time, and  $\nabla$  represents a  
 25 gradient in the spatial domain  $\Omega \subseteq \mathbb{R}^d$  with  $1 \leq d \leq 3$  being the space-dimension. The  
 26 BE signifies the fact that the pdf changes due to the free-streaming of the gas molecules  
 27 and the inter-molecular collisions—the collision operator  $Q$  models the inter-particle  
 28 collisions, and the transport operator  $\partial_t + \xi \cdot \nabla$  models the free-streaming of the gas  
 29 molecules.

30 In practical applications, one is not interested in the fine details of a pdf but in the  
 31 macroscopic quantities like density, velocity, temperature, etc. These quantities can  
 32 be recovered by taking the velocity-moments of the pdf. This motivates the method-  
 33 of-moments (MOM) approach, where, rather than directly solving the BE, we solve for  
 34 a finite number of moments of the pdf. The velocity-moments of the BE provide the  
 35 governing equation for the moments of  $f(x, t, \cdot)$ , or the so-called moment equations.  
 36 However, a finite set of moment equations is not closed—the flux term  $(\xi \cdot \nabla f)$  results  
 37 in a moment of degree higher than that included in the moment set. Nevertheless, one  
 38 can close the moment equations by solving the following moment-closure problem.

39 (1.2) Moment-closure problem: given a set of moments, find the underlying pdf.

41 There are infinitely many solutions to the moment-closure problem [21]. To single-  
 42 out a unique solution, one can introduce an optimality criterion by minimizing a

---

\*Submitted to the editors xxxx

**Funding:** N.S is supported by the German Federal Ministry for Economic Affairs and Energy (BMWi) in the joint project "MathEnergy - Mathematical Key Technologies for Evolving Energy Grids", sub-project: Model Order Reduction (Grant number: 0324019B).

<sup>†</sup>Corresponding author, Max Planck Institute for Dynamics of Complex Technical Systems, Sandtorstr 1, 39106, Magdeburg, Germany, [sarna@mpi-magdeburg.mpg.de](mailto:sarna@mpi-magdeburg.mpg.de).

43 strictly convex functional of the pdf. We choose this functional to be the L2-norm of  
 44 the pdf. Our choice is motivated by a discontinuous Galerkin (DG) discretization of  
 45 the velocity domain that we interpret as an L2-minimization problem with moment  
 46 constraints—later sections provide further clarification.

47 A major drawback of L2-minimization (and so of a DG-discretization [3]) is that it  
 48 does not penalize the negativity of a solution—for the same reason, a Hermite spectral  
 49 method proposed in [15] does not ensure positivity. This is undesirable given that we  
 50 are approximating a pdf that is positive by definition. There is ample numerical and  
 51 theoretical evidence supporting the claim that a positive solution to a moment-closure  
 52 problem better approximates a pdf—see the different works on positive moment-  
 53 methods [1, 8, 10, 18, 20, 22, 30, 37]. Furthermore, in theory, a negative solution to a  
 54 moment-closure problem can result in a negative density and temperature, resulting  
 55 in a breakdown of the solution algorithm. For this reason, we enforce positivity  
 56 constraints on our L2-minimization problem. This results in a quadratic optimization  
 57 problem with moments and positivity constraints.

58 For the robustness of the algorithm, the feasibility of the quadratic optimization  
 59 problem is imperative. We show that a CFL-type condition ensures (i) the feasibility  
 60 of the optimization problem and (ii) the L2-stability of the moment approximation—  
 61 we insist that stability is crucial in analyzing the convergence of a moment approx-  
 62 imation [24, 26]. A proof for both these properties hinges on relating our moment  
 63 approximation to a discrete-velocity-method (DVM). We emphasize that our proof is  
 64 general in the sense that it is independent of the objective functional being minimized  
 65 to single-out a unique solution to the moment-closure problem.

66 Other than L2-minimization (with positivity constraints) one can consider entropy-  
 67 minimization. Despite the many favourable properties (see [16, 19, 20, 29, 31]), it is  
 68 challenging to compute an entropy-minimization based closure. A few reasons for this  
 69 are as follows. Firstly, to perform entropy-minimization one usually performs Newton  
 70 iterations where in every iteration one inverts the Hessian of the objective functional.  
 71 This Hessian (despite the adaptivity of basis proposed in [5]) can become severely  
 72 ill-conditioned—particularly inside shocks and for large moment sets—leading to a  
 73 slow (or no) convergence of the Newton solver [29, 30]. Secondly, in every Newton  
 74 iteration, one needs to compute integrals over the  $d_\xi$ -dimensional velocity domain.  
 75 An analytical expression for these integrals is usually unavailable and one seeks a  
 76 numerical approximation via some quadrature routine. The number of these quad-  
 77 rature points can grow drastically with  $d_\xi$ , making the solution algorithm expensive  
 78 for multi-dimensional applications [8, 29, 30]. For instance, the number of tensorized  
 79 Gauss-Legendre quadrature points grow as  $\mathcal{O}(N^{d_\xi})$ , where  $N$  is the number of quad-  
 80 rature points in one direction.

81 Replacing entropy minimization by L2-minimization (with positivity constraints)  
 82 does not necessarily solves the two problems mentioned above. We use the interior-  
 83 convex-set algorithm to perform L2-minimization and even for problems with strong  
 84 shocks and large moment sets, we did not encounter issues with the conditioning of  
 85 the Hessian. Our results suggest that L2-minimization could be an alternative to  
 86 entropy-minimization for flow regimes where entropy-minimization losses robustness.  
 87 Furthermore, since L2-minimization is robust for large moment sets, it is appealing for  
 88 an adaptive approach where depending upon the accuracy requirements, the moment  
 89 set can change locally in the space-time domain [2, 38].

90 We note that although our L2-minimization procedure is robust, to approximate  
 91 the integrals, we use tensorized Gauss-Legendre quadrature points in the velocity  
 92 domain, which, we expect, makes L2-minimization expensive. Specialized quadrature

93 points can make both L2 and entropy minimization efficient [8]. However, these  
 94 quadrature points do not guarantee the feasibility of the minimization problem—a  
 95 property we consider crucial for the robustness of the solution algorithm. To tackle  
 96 infeasible problems, one can try regularizing the minimization problem by relaxing  
 97 the moment constraints [4]. The use of a specialized quadrature with a regularized  
 98 minimization problem is an interesting direction to pursue and we plan to consider it  
 99 in the future.

100 We acknowledge that our work draws inspiration from the positive  $PN$  closure  
 101 proposed in [18] for the radiative transport equation. Indeed, we solve a similar  
 102 optimization problem as that solved by the positive  $PN$  closure. Nevertheless, our  
 103 work differs from [18] in the following ways. Firstly, unlike the linear isotropic colli-  
 104 sion operator considered in [18], we consider the non-linear Boltzmann-BGK operator  
 105 that we discretize using entropy-minimization to ensure mass, momentum and energy  
 106 conservation. Secondly, using the solution of the optimization problem, to close the  
 107 moment system, authors in [18] perform a spherical harmonics based velocity recon-  
 108 struction of the pdf. Our framework suggests that such a reconstruction is not needed  
 109 if one uses the same quadrature points to compute moments in the moment equations  
 110 and to solve the minimization problem. Thirdly, through numerical experiments, we  
 111 study the convergence of our moment approximation and compare it to the DVM.  
 112 These studies were not performed in [18]. Lastly, we establish robust (under van-  
 113 ishing Knudsen limit) L2-stability estimates for our moment approximation. Let us  
 114 emphasize that to the best of our knowledge, for gas transport applications, none of  
 115 the previous works consider L2-minimization based moment-closures with positivity  
 116 constraints.

117 We have organized the rest of the article as follows. In [Section 2](#) we discuss  
 118 our moment approximation and the details of the BE. In [Section 3](#) we discuss the  
 119 space-time discretization of the moment equations, the feasibility of the optimization  
 120 problem, and the stability of the moment approximation. In [Section 4](#) we extend  
 121 our framework to multi-dimensional problems, and in [Section 5](#) we perform numerical  
 122 experiments.

123 **2 Moment Approximation** Throughout this section we consider a one di-  
 124 mensional space-velocity domain i.e.,  $d = d_\xi = 1$  in (1.1). An extension to multi-  
 125 dimensions is straightforward and is discussed in [Section 4](#). We start by discussing a  
 126 positive L2-minimization based moment-closure and use it later to define a moment  
 127 approximation for the BE.

128 **2.1 A positive L2-method-of-moments (pos-L2-MOM)** Consider a  $m$ -th  
 129 order polynomial in  $\xi$  given as  $p_m(\xi) := \xi^m$ . Collect all the different  $p_m(\xi)$  upto some  
 130 order  $(M - 1) \in \mathbb{N}$  in a vector  $P_M(\xi)$  given as

$$\begin{aligned}
 131 & \\
 132 & (2.1) \quad P_M(\xi) := (p_0(\xi), \dots, p_{M-1}(\xi))^T,
 \end{aligned}$$

133 where  $(\cdot)^T$  represents the transpose of a vector. For a function  $\xi \mapsto g(\xi) \in \mathbb{R}$ , we  
 134 introduce the shorthand notation

$$\begin{aligned}
 135 & (2.2) \quad \langle g \rangle := \int_{\mathbb{R}} g(\xi) d\xi. \\
 136 &
 \end{aligned}$$

137 Note that the definition of  $P_M$  implies that the vector  $\langle P_M g \rangle$  contains the first  $M$   
 138 moments of  $g$ .

139 For some moment vector  $\lambda \in \mathbb{R}^M$ , consider the mathematical formulation of the  
 140 moment-closure problem described earlier in the introduction

$$141 \quad (2.3) \quad \text{Find } g_M : \langle P_M g_M \rangle = \lambda.$$

143 Even for a realizable moment vector  $\lambda$  (i.e., there exists a  $g^* > 0$  such that  $\lambda =$   
 144  $\langle P_M g^* \rangle$ ), the above problem can have infinitely many solutions [21]. To single-out  
 145 a unique solution, we use L2-minimization as an optimality criterion. Since L2-  
 146 minimization does not penalize negativity and since we prefer a positive solution  
 147 to the moment-closure problem, we explicitly enforce a positivity constraint. This  
 148 result in an optimization problem given as

$$149 \quad (2.4) \quad g_M := \arg \min_{g^* \in L^2(\mathbb{R})} \frac{1}{2} \|g^*\|_{L^2(\mathbb{R})}^2 : \langle P_M g^* \rangle = \lambda, g^* > 0.$$

151 In the above minimization problem, as yet, it is unclear how to enforce the pos-  
 152 itivity constraint almost everywhere on  $\mathbb{R}$ . To tackle this problem, we consider the  
 153 following two steps—we refer to [18, 29, 30] for similar steps related to the minimum-  
 154 entropy closure and the positive PN closure.

- 155 1. *Truncate the velocity domain:* We truncate the velocity domain  $\mathbb{R}$  to  $\Omega_\xi :=$   
 156  $[\xi_{\min}, \xi_{\max}]$ . A decent estimate for  $\xi_{\max/\min}$  follows from the velocity and the  
 157 temperature field of the gas and is discussed later in [Subsection 2.4](#). The  
 158 same sub-section discusses the pros and cons associated with truncating the  
 159 velocity domain.
- 160 2. *Positivity constraints on quadrature points:* To perform the integrals in the  
 161 minimization problem, we use some quadrature points defined over  $\Omega_\xi$ . We  
 162 enforce the positivity constraints only over these quadrature points. Although  
 163 our framework is valid for any set of space-time-independent quadrature  
 164 points, for completeness, we consider  $N$  Gauss-Legendre quadrature points  
 165 and we denote their weights and abscissas by  $\{\omega_i\}_i$  and  $\{\xi_i\}_i$ , respectively.  
 166 Using the quadrature points, for some function  $\xi \mapsto g(\xi) \in \mathbb{R}$ , we define

$$167 \quad (2.5) \quad \langle g \rangle \approx \langle g \rangle_N := \sum_{i=1}^N \omega_i g(\xi_i).$$

169 For convenience, with  $W(g) \in \mathbb{R}^N$  we represent a vector that collects all the  
 170 values of  $g$  at the quadrature points i.e.,

$$171 \quad (2.6) \quad (W(g))_i := g(\xi_i), \quad \forall i \in \{1, \dots, N\}.$$

173 With the above two simplifications, the optimization problem in (2.4) transforms  
 174 to an optimization problem for  $W(g_M)$  given as

$$175 \quad (2.7) \quad W(g_M) = \arg \min_{W^* \in \mathbb{R}^N} \frac{1}{2} \|W^*\|_2^2 : \underline{ALW^*} = \lambda, W^* > 0.$$

177 To write down the moment constraint (the underlined term) in the above problem,  
 178 we have used the relation

$$179 \quad (2.8) \quad \langle P_M g^* \rangle \approx \langle P_M g^* \rangle_N = ALW(g^*),$$

181 where the matrices  $A \in \mathbb{R}^{M \times N}$  and  $L \in \mathbb{R}^{N \times N}$  are given as

$$182 \quad (2.9) \quad A := (P_M(\xi_1), \dots, P_M(\xi_N)), \quad L_{ij} = \begin{cases} \omega_i, & i = j \\ 0, & i \neq j \end{cases}.$$

184 Thus,  $L$  is a diagonal matrix containing the quadrature weights  $\{\omega_i\}$  at its diagonal,  
 185 and  $A$  is a Vandermonde matrix. Note that in (2.7), for notational simplicity, we  
 186 defined  $W^* = W(g^*)$ .

187 **REMARK 1** (A DG discretization). *To see the similarity between the pos-L2-*  
 188 *MOM and a DG velocity space discretization and understand our motivation behind*  
 189 *considering L2-minimization, consider the optimization problem*

$$190 \quad g_M^{DG} := \arg \min_{g^* \in L^2(\Omega_\xi)} \frac{1}{2} \|g^*\|_{L^2(\Omega_\xi)}^2 : \int_{\Omega_\xi} P_M g^* d\xi = \lambda.$$

191  
 The above problem is a continuous-in-velocity analogue of (2.4) but without positivity  
 constraints. Using the first order-optimality conditions, one can conclude that a solu-  
 tion to the above problem is given as (see page-2611 of [18] for a proof related to the  
 PN closure)

$$g_M^{DG} = \alpha^T P_M,$$

192 where  $\alpha$  is a vector of expansion coefficients related linearly to the moment vector  
 193  $\lambda$ —the exact form of  $\alpha$  is not important here. The above expansion is the same as  
 194 the DG velocity discretization proposed in [3]. Thus, one can interpret pos-L2-MOM  
 195 as a DG velocity discretization with positivity constraints. Note that the optimization  
 196 problem corresponding to  $g_M^{DG}$  does not penalize the negativity of a solution therefore,  
 197  $g_M^{DG}$  is not necessarily positive on the quadrature points.

198 **REMARK 2** (A Hermite expansion). *One can also interpret a Hermite approxima-*  
 199 *tion to a pdf as a solution to a weighted L2-minimization problem—we refer to [15, 43]*  
 200 *for an exhaustive discussion on Hermite expansions. Let  $p_m(\xi)$  denote the  $m$ -th order*  
 201 *Hermite polynomial  $He_m(\xi)$ . Normalize the Hermite polynomials such that they are*  
 202 *orthogonal under the inner-product of the weighted L2-space  $L^2(\mathbb{R}, \exp(-\xi^2/2))$ . Let*  
 203  *$P_M$  be as defined in (2.1). Note that instead of monomials, the vector  $P_M(\xi)$  now*  
 204 *contains Hermite polynomials.*

205 Consider a weighted L2-minimization problem given as

$$206 \quad g_M^H := \arg \min_{g^* \in L^2(\mathbb{R}, \exp(\xi^2/2))} \frac{1}{2} \|g^*\|_{L^2(\mathbb{R}, \exp(\xi^2/2))}^2 : \langle P_M g^* \rangle = \lambda.$$

207  
 Note that as compared to a DG approximation, in the above optimization problem, we  
 did not truncate the velocity domain. One can show that the solution to the above  
 minimization problem is given as

$$g_M^H = \lambda^T P_M \exp(-\xi^2/2),$$

208 which is similar to the Hermite spectral method proposed in [15]. Using the same  
 209 methodology as for the L2-minimization, one can impose positivity constraints in the  
 210 above minimization problem and enforce them on a set of Gauss-Hermite quadra-  
 211 ture points. We leave the development of a positive weighted L2-minimization based  
 212 moment method as a part of our future work.

213 **2.1.1 Feasibility of the positive L2-minimization** If there exists a  $z > 0$   
 214 such that  $\lambda = ALz$  then the optimization problem in (2.7) is feasible with the feasible  
 215 point  $W^* = z$ . We collect this simple, but noteworthy, result as follows. We first  
 216 define a set of realizable moments

$$217 \quad (2.10) \quad R := \{\lambda : \lambda \in \mathbb{R}^M, \lambda = ALz, z > 0\}.$$

219 Using  $R$ , we collect our statement related to the feasibility of the optimization prob-  
 220 lem.

221 **LEMMA 2.1** (Feasibility of the optimization problem). *The optimization problem*  
 222 *in (2.7) is feasible if  $\lambda \in R$ .*

Note that for a given  $\lambda \in R$ , the number of feasible points of the optimization  
 problem vary depending upon the value of  $N$  relative to  $M$ . Let  $z > 0$  be such that  
 $\lambda = ALz$ . A feasible point  $W^*$  of the optimization problem (2.7) is a positive solution  
 of the linear system

$$ALW^* = ALz.$$

223 Since  $AL$  is a full-rank matrix ( $A$  is a Vandermonde matrix and the Gauss-Legendre  
 224 quadrature weights are positive), the above linear system has a unique solution  $W^* =$   
 225  $z$  for  $N \leq M$ . Thus, the optimization problem has a single feasible point for  $N \leq M$ .  
 226 In contrast, the above linear system has infinitely many positive solutions for  $N > M$ ,  
 227 resulting in infinitely many feasible points.<sup>1</sup>

228 The above discussion indicates that for  $N \leq M$ , we do not need to perform L2-  
 229 minimization. A unique positive  $W(g_M)$  can be recovered by solving the moment  
 230 constraint  $ALW(g_M) = \lambda$ . However, for  $N \leq M$ , a moment-based approach is  
 231 meaningless because we can directly compute  $W(g_M)$  using a discrete-velocity-method  
 232 (DVM). Since  $N \leq M$ , this would be less expensive than first computing  $\lambda$  and  
 233 then computing  $W(g_M)$  using the optimization problem. Therefore, in the following  
 234 discussion we only consider  $N > M$ . The discussion here becomes clearer when we  
 235 later relate our moment approximation to a DVM.

236 **REMARK 3** (Practical considerations while choosing  $N$ ). *Practical considera-*  
 237 *tions suggest a compromise between small and large values of  $N$ . We use an inter-*  
 238 *convex-set algorithm to solve the minimization problem in (2.7). A crude estimate*  
 239 *for the complexity of this algorithm is  $\mathcal{O}(N^3)$  [42]. Thus, choosing a large value of*  
 240  *$N$  increases the computational cost of solving the optimization problem, which, as we*  
 241 *discuss later, is the most expensive part of our moment approximation. On the con-*  
 242 *trary, we do not want  $N$  to be so small that the error (measured in some norm) in*  
 243 *our moment approximation is dominated by the error in our quadrature approxima-*  
 244 *tion. Numerical experiments suggest that choosing  $N$  between  $2M$  and  $5M$  is a good*  
 245 *compromise between accuracy and efficiency.*

246 **2.2 The Boltzmann Equation (BE)** Equipping the BE with initial and  
 247 boundary data provides

$$248 \quad (2.11) \quad \begin{aligned} \mathcal{L}(f) &= 0 \text{ on } \Omega \times D \times \mathbb{R}, & f(\cdot, t = 0, \cdot) &= f_0 \text{ on } \Omega \times \mathbb{R}, \\ f &= f_{in} \text{ on } \partial\Omega_- \times D. \end{aligned}$$

<sup>1</sup>Let  $W^*$  be a solution to  $ALW^* = ALz$ . Let  $v$  be an element of the null-space of  $AL$ —since  $AL$  is a flat matrix, its null-space is non-empty. Then, for all  $\beta$  such that  $\min_i(\beta v_i) > -\min_i(w_i)$ , we find that  $W^* + \beta v$  is also a feasible point.

249 Above, the spatial domain is given as  $\Omega := [x_{\min}, x_{\max}]$ , and  $\partial\Omega_-$  is the inflow part  
 250 of the boundary that reads

$$251 \quad (2.12) \quad \partial\Omega_- := \{(x, \xi) : \xi \cdot n(x) \leq 0, x \in \partial\Omega\},$$

253 where  $n(x)$  is a unit normal at  $x \in \partial\Omega$  that points out of the domain. For simplicity,  
 254 we consider only inflow type boundary conditions and not wall boundary conditions  
 255 i.e.,  $f_{in}$  is the given data and is independent of the solution  $f$  [12]. An inflow type  
 256 boundary simplifies our result related to the stability of the moment approximation  
 257 discussed later. With some additional technical details, one can extend our stability  
 258 result to solid-wall boundaries—see [28] for stability results related to a solid-wall  
 259 boundary for a Grad’s moment method.

260 We normalise  $f$  such that the density  $\rho$ , the velocity  $v$  and the temperature  $\theta$  (in  
 261 energy units) reads

$$262 \quad (2.13) \quad \left( \begin{array}{c} \rho(x, t) \\ \rho(x, t)v(x, t) \\ \rho(x, t)(\theta(x, t) + v(x, t)^2) \end{array} \right) := \langle P_{\text{cons}}f(x, t, \cdot) \rangle, \quad P_{\text{cons}}(\xi) := \left( \begin{array}{c} 1 \\ \xi \\ \xi^2 \end{array} \right).$$

264 Note that for  $M \geq 3$ ,  $P_{\text{cons}}(\xi)$  is nothing but the first three entries of  $P_M(\xi)$ .

265 We consider a Boltzmann-BGK collision operator given as

$$266 \quad (2.14) \quad Q(f(x, t, \xi)) := \frac{1}{\tau(x, t)}(f_{\mathcal{M}}(x, t, \xi) - f(x, t, \xi)),$$

268 where the collision frequency  $\tau(x, t)^{-1}$  reads  $\tau(x, t)^{-1} := C\rho(x, t)\theta(x, t)^{1-\omega}$  with  $\omega$   
 269 begin the exponent in the viscosity law of the gas [13]. The collision operator rep-  
 270 represents the fact that the pdf  $f(x, t, \cdot)$  is pushed towards the Maxwell-Boltzmann pdf  
 271  $f_{\mathcal{M}}(x, t, \cdot)$  given as

$$272 \quad (2.15) \quad f_{\mathcal{M}}(x, t, \xi) := \frac{\rho(x, t)}{\sqrt{2\pi\theta(x, t)}} \exp\left(-\frac{(\xi - v(x, t))^2}{2\theta(x, t)}\right).$$

274 We can also interpret  $f_{\mathcal{M}}$  as a solution to an entropy-minimization problem. Out  
 275 of all the pdfs that have the same mass, momentum and energy as  $f(x, t, \cdot)$ , the pdf  
 276  $f_{\mathcal{M}}(x, t, \cdot)$  is the one that minimizes the Boltzmann’s entropy. Equivalently,

$$277 \quad (2.16) \quad f_{\mathcal{M}}(x, t, \cdot) = \arg \min_{f^*(\xi) \geq 0} \{ \langle f^* \log(f^*) \rangle : \langle P_{\text{cons}}f^* \rangle = \langle P_{\text{cons}}f(x, t, \cdot) \rangle \}.$$

279 Later, we use the above interpretation of  $f_{\mathcal{M}}$  to discretize it on a velocity grid. A  
 280 noteworthy property of  $Q(f)$  is its collision invariance i.e.,  $\langle P_{\text{cons}}Q(f) \rangle = 0$  for all  $f$  in  
 281 the domain of  $Q$ . This ensures that the BE conserves mass, momentum and energy.  
 282 By considering  $M \geq 3$ , which ensures that  $P_{\text{cons}}(\xi)$  is contained in the vector  $P_M(\xi)$ ,  
 283 and by carefully discretizing the collision operator as in [22], we will ensure that our  
 284 moment system also conserves these quantities.

285 **2.3 Moment equations** We present a moment approximation to the BE based  
 286 upon the pos-L2-MOM described in Subsection 2.1. To derive a governing equation  
 287 for the moments  $\langle P_M f(x, t, \cdot) \rangle$ , we take (discrete) velocity moments of the BE given  
 288 in (2.11) to find

$$289 \quad (2.17) \quad \partial_t \langle P_M f(x, t, \cdot) \rangle_N + \partial_x \langle P_M \xi f(x, t, \cdot) \rangle_N = \langle P_M Q(f(x, t, \cdot)) \rangle_N.$$

291 Recall that  $\langle \cdot \rangle_N$  is as defined in (2.5) and is a numerical approximation to the integral  
 292  $\langle \cdot \rangle$ .

293 The above system of equations is not closed—the underlined flux-term contains a  
 294  $M$ -order moment that is not contained in the moment vector  $\langle P_M f(x, t, \cdot) \rangle_N$ . To close  
 295 the system of equations, using the moments  $\langle P_M f(x, t, \cdot) \rangle_N$ , we need to approximate  
 296 the values of  $f(x, t, \cdot)$  at the quadrature points i.e., we need to approximate the vector  
 297  $W(f(x, t, \cdot))$  using the moments  $\langle P_M f(x, t, \cdot) \rangle_N$ . We approximate  $W(f(x, t, \cdot))$  by  
 298  $W(f_M(x, t, \cdot))$ . To compute  $W(f_M(x, t, \cdot))$ , we use the L2-minimization problem given  
 299 in (2.7) with the moment vector  $\lambda$  set to  $\langle P_M f(x, t, \cdot) \rangle_N$ . This results in the following  
 300 closed set of moment equations

$$301 \quad (2.18) \quad \partial_t \langle P_M f_M \rangle_N + \partial_x \langle P_M \xi f_M \rangle_N = \frac{1}{\tau} (\langle P_M f_{M,N} \rangle_N - \langle P_M f_M \rangle_N) \text{ on } \Omega \times D,$$

$$\langle P_M f_M(t=0) \rangle_N = \langle P_M f_0 \rangle_N \text{ on } \Omega.$$

302 Our space-time discretization [Subsection 3.2](#) will discuss the boundary discretization.  
 303 Let us emphasize again that to compute the flux term  $\langle P_M \xi f_M(x, t, \cdot) \rangle_N$ , we only need  
 304 the value of  $W(f_M(x, t, \cdot))$ , which are available after solving the L2-minimization  
 305 problem.

306 The pdf  $f_{M,N}$  is an approximation to the Maxwell-Boltzmann pdf  $f_M$  and is such  
 307 that  $W(f_{M,N})$  is a solution to an entropy-minimization problem given as [\[22\]](#)

$$308 \quad (2.19) \quad W(f_{M,N}(x, t, \cdot)) = \arg \min_{W^* \in \mathbb{R}_{>0}^N} \left\{ \sum_i w_i^* \log(w_i^*) \omega_i : A_{\text{cons}} L W^* = \langle P_{\text{cons}} f_M(x, t, \cdot) \rangle_N \right\}.$$

310 The above problem is a discrete-in-velocity analogue of the entropy minimization  
 311 problem given in (2.16). Furthermore, the moment constraints in the minimization  
 312 problem ensure that the moment system (2.18) conserves mass, momentum and en-  
 313 ergy.

314 **2.4 Computing the velocity cut-off** Recall that we truncate the velocity  
 315 domain  $\mathbb{R}$  to  $\Omega_\xi = [\xi_{\min}, \xi_{\max}]$ . We use the same technique as a DVM to compute the  
 316 velocity cut-off  $\xi_{\max/\min}$ . The technique is summarised as follows—for further details,  
 317 we refer to [\[7, 22\]](#) and the references therein. Estimating  $\xi_{\max/\min}$  using the velocity  
 318 and the temperature of the gas provides

$$319 \quad (2.20) \quad \xi_{\min} := \inf_{(x,t) \in \Omega \times D} \left( v(x, t) - c \sqrt{\theta(x, t)} \right),$$

$$\xi_{\max} := \sup_{(x,t) \in \Omega \times D} \left( v(x, t) + c \sqrt{\theta(x, t)} \right).$$

320 From arguments in statistical mechanics, a value of  $c$  between 3 and 4 is desirable.  
 321 Choosing  $c = 3.5$  balances accuracy and computational cost. During numerical ex-  
 322 periments, we compute a reference solution using a DVM. To ensure that the DVM  
 323 solution is sufficiently refined, we perform a convergence study by first estimating  
 324  $\xi_{\max/\min}$  using the initial data and the above formulae and then increasing  $\xi_{\max}$  (and  
 325 decreasing  $\xi_{\min}$ ) till the relative error between two subsequent refinements drops be-  
 326 low an acceptable value. We use  $\xi_{\max}$  from the last refinement cycle for both the  
 327 DVM and the pos-L2-MOM—[Section 5](#) provides further details. In practical appli-  
 328 cations, one can estimate  $v(x, t)$  and  $\theta(x, t)$  using a Navier-Stokes solver, which is  
 329 usually much cheaper than a BE solver [\[7\]](#).



330 **REMARK 4** (Pros and cons of a space-time-independent  $\xi_{\max}$ ). *Our choice of  $\xi_{\max}$*   
 331 *(and  $\xi_{\min}$ ) is space-time-independent, which has both positive and negative conse-*  
 332 *quences. Such a velocity cut-off can be accurate only if, on the entire space-time*  
 333 *domain,  $f(x, t, \cdot)$  is sufficiently small outside of  $\Omega_\xi$ . In terms of the macroscopic quan-*  
 334 *tities, we can expect to be accurate only for flows with a velocity and a temperature*  
 335 *inside a certain range [22]. Let us mention that we share these negative consequences*  
 336 *of truncating a velocity domain with the DVM and the entropy-minimization based clo-*  
 337 *sures [22, 30]. On the positive side, as we discuss later, with a space-time-independent*  
 338  *$\xi_{\max}$  it is straightforward to ensure the feasibility of the optimization problem in (2.7).*  
 339 *Furthermore, the stability of the moment equations that we establish later can also be*  
 340 *attributed to  $\xi_{\max}$  being fixed in space-time.*

341 **REMARK 5** (A space-time-dependent  $\xi_{\max}$ ). *To overcome the limitations men-*  
 342 *tioned in the previous remark, similar to [9], one can introduce space-time-dependence*  
 343 *in  $\xi_{\max}$ . We failed to introduce this dependence without sacrificing the feasibility of the*  
 344 *optimization problem (2.7) and the stability result discussed later. To overcome the*  
 345 *feasibility issue, one can try modifying the optimization problem by regularizing it [4].*  
 346 *The regularization adds the moment constraint as a penalty term and tries to mini-*  
 347 *mize both the L2-norm of the pdf and the error in satisfying the moment constraint.*  
 348 *As for the stability, it is unclear how one can ensure it with a space-time-dependent*  
 349  *$\xi_{\max}$ . We leave the development of pos-L2-MOM with space-time adaptive  $\xi_{\max}$  as a*  
 350 *part of our future work.*

### 351 **3 Space-time discretization**

352 **3.1 Preliminaries** We partition  $\Omega = [x_{\min}, x_{\max}]$  into  $N_x$  intervals given as

$$\begin{aligned}
 353 \quad (3.1) \quad \Omega &= \bigcup_{i=1}^{N_x} \mathcal{I}_i, \quad \mathcal{I}_i = [x_{i-1/2}, x_{i+1/2}], \\
 354
 \end{aligned}$$

355 where  $x_{1/2} = x_{\min}$  and  $x_{N_x+1/2} = x_{\max}$ . With  $\{t_i\}_{i=1, \dots, K} \subset D$  we represent a set of  
 356 discrete time instances such that  $0 = t_1 < t_2 \dots < t_K = T$ . For simplicity of notation,  
 357 we assume that all the space and the time intervals are of the same size  $\Delta x$  and  $\Delta t$ ,  
 358 respectively. An extension to non-uniform space-time grids is straightforward. We  
 359 denote the finite volume (FV) approximation of  $\langle P_M f_M(x, t, \cdot) \rangle$  and  $\langle P_M f_{\mathcal{M}, N}(x, t, \cdot) \rangle$   
 360 in the  $i$ -th cell and at the  $k$ -th time instance by

$$\begin{aligned}
 361 \quad (3.2) \quad \langle P_M f_i^k \rangle_N &\approx \frac{1}{\Delta x} \int_{\mathcal{I}_i} \langle P_M f_M(x, t_k, \cdot) \rangle_N dx, \\
 \langle P_M f_{\mathcal{M}, i}^k \rangle_N &\approx \frac{1}{\Delta x} \int_{\mathcal{I}_i} \langle P_M f_{\mathcal{M}, N}(x, t_k, \cdot) \rangle_N dx.
 \end{aligned}$$

362 Above,  $f_{\mathcal{M}, N}$  is the discretization of the Maxwell-Boltzmann distribution introduced  
 363 in (2.16) and for notational simplicity, we have suppressed the  $M$  dependence in  $f_i^k$ .

364 Using the matrix  $A$  and  $L$  given in (2.9), we can express the space-time discrete  
 365 moments in a matrix-vector product form as

$$366 \quad (3.3) \quad \langle P_M f_i^k \rangle_N = ALW(f_i^k), \quad \langle P_M f_{\mathcal{M}, i}^k \rangle = ALW(f_{\mathcal{M}, i}^k),$$

367 where  $W(f_i^k)$  and  $W(f_{\mathcal{M}, i}^k)$  are the FV-approximations to  $W(f_M(x, t_k, \cdot))$  and  
 368  $W(f_{\mathcal{M}}(x, t_k, \cdot))$ , respectively, in the  $i$ -th cell and at the  $k$ -th time step. For later  
 369 convenience, with  $f_{M, N_x}$  we represent an FV approximation to  $f_M$  defined as

$$370 \quad (3.4) \quad f_{M, N_x}(x, t_k, \xi) = f_i^k(\xi), \quad \forall x \in \mathcal{I}_i, k \in \{1, \dots, K\}, \xi \in \{\xi_i\}_i.$$

372 **3.2 Evolution scheme** The evolution scheme consists of four steps outlined  
 373 below. We present these steps for some representative  $t = t_k$ . Each step is repeated  
 374 from  $k = 1$  to  $k = K - 1$ . For  $k = 1$ , we initialize with

$$375 \quad (3.5) \quad \langle P_M f_i^k \rangle_N = \frac{1}{\Delta x} \int_{\mathcal{I}_i} \langle P_M f_0(x, \cdot) \rangle_N dx, \quad \forall i \in \{1, \dots, N_x\},$$

377 where  $f_0$  is the initial data in (2.11). We approximate the above space integral with  
 378 10 Gauss-Legendre quadrature points in each cell.

- 379 1. *Entropy-minimization step:* Using the conserved moments  $\{\langle P_{\text{cons}} f_i^k \rangle_N\}_i$ ,  
 380 solve the entropy minimization problem in (2.19). This provides the discrete  
 381 Maxwell-Boltzmann pdf  $\{f_{\mathcal{M},i}^k\}_i$ .
- 382 2. *Collision step:* With the output of the previous step, perform collisions with  
 383 an implicit Euler time-stepping scheme. At some intermediate  $t_{k^*} \in (t_k, t_{k+1})$   
 384 and for all  $i \in \{1, \dots, N_x\}$ , this provides [14]

$$385 \quad (3.6) \quad \frac{\langle P_M f_i^{k^*} \rangle_N - \langle P_M f_i^k \rangle_N}{\Delta t} = \frac{1}{\tau(x_i, t_{k^*})} \left( \langle P_M f_{\mathcal{M},i}^{k^*} \rangle_N - \langle P_M f_i^{k^*} \rangle_N \right).$$

387 There is an explicit solution to the above implicit collision step. Since the  
 388 collision step preserves mass, moment and energy and since the solution of the  
 389 entropy-minimization problem (2.19) is unique for a given set of conserved  
 390 moments, we find  $W(f_{\mathcal{M},i}^{k^*}) = W(f_{\mathcal{M},i}^k)$ . This implies that  $\langle P_M f_{\mathcal{M},i}^{k^*} \rangle_N =$   
 391  $\langle P_M f_{\mathcal{M},i}^k \rangle_N$ , which provides

$$392 \quad (3.7) \quad \begin{aligned} \langle P_M f_i^{k^*} \rangle_N &= \frac{1}{1 + \Delta t / \tau(x_i, t_{k^*})} \langle P_M f_i^k \rangle_N \\ &\quad + \frac{\Delta t / \tau(x_i, t_{k^*})}{1 + \Delta t / \tau(x_i, t_{k^*})} \langle P_M f_{\mathcal{M},i}^k \rangle_N. \end{aligned}$$

- 393 3. *Optimization step:* Using the moments  $\{\langle P_M f_i^{k^*} \rangle_N\}_i$ , compute the weights  
 394  $\{W(f_i^{k^*})\}_i$  by solving the optimization problem in (2.7).
- 395 4. *Transport step:* Using the output of the previous step, perform the transport  
 396 step given as

$$397 \quad (3.8) \quad \begin{aligned} \frac{\langle P_M f_i^{k+1} \rangle_N - \langle P_M f_i^{k^*} \rangle_N}{\Delta t} &= -\frac{1}{\Delta x} \left( \mathcal{F}(W(f_{i+1}^{k,*}), W(f_i^{k,*})) \right. \\ &\quad \left. - \mathcal{F}(W(f_i^{k,*}), W(f_{i-1}^{k,*})) \right). \end{aligned}$$

398 To impose boundary conditions, for  $i = 1$ , set  $W(f_{i-1}^{k,*}) = W(f_{in}(t, \cdot))$  and for  
 399  $i = N_x$ , set  $W(f_{i+1}^{k,*}) = W(f_{in,N}(t, \cdot))$ , where  $f_{in}$  is the boundary data given  
 400 in (2.11). Above,  $\mathcal{F} : \mathbb{R}^N \times \mathbb{R}^N \rightarrow \mathbb{R}^M$  is the numerical flux and since we  
 401 consider a kinetic upwind numerical flux, it reads [1]

$$402 \quad (3.9) \quad \mathcal{F}(W_1, W_2) := \frac{1}{2} (AL(\Xi - |\Xi|)W_1 + AL(\Xi + |\Xi|)W_2).$$

404 Above,  $A$  and  $L$  are the two matrices defined in (2.9). The matrix  $\Xi$  is  
 405 a diagonal matrix with the locations of the quadrature points  $\{\xi_i\}_i$  at its  
 406 diagonal. Furthermore,  $|\Xi|$  is a matrix representing the absolute value of  $\Xi$  in  
 407 the sense that  $(|\Xi|)_{ij} = |\Xi_{ij}|$ . For clarity, to express  $\mathcal{F}$  in a standard kinetic  
 408 upwind flux form, note that  $AL(\Xi \pm |\Xi|)W_1 = \langle P_M(\xi \pm |\xi|)f_1 \rangle_N$ .

409 **REMARK 6** (Space-time locality of the optimization step). *The optimization step*  
 410 *(and also the entropy minimization step) is a local in space-time operation. We loop*  
 411 *over each spatial cell, solve the optimization problem, add the local contributions to*  
 412 *the numerical flux and move over to the next cell. Therefore, at any given point in*  
 413 *time, we store only the moments in all the spatial cells and not the values of the pdf*  
 414 *at the quadrature points. This results in a drastic reduction in memory consumption*  
 415 *since, in practice, the number of quadrature points are much larger than the number*  
 416 *of moments—see [29, 30] for a similar comment related to a maximum-entropy clo-*  
 417 *sure. Let us emphasize that in comparison, a DVM stores the values of the pdf at the*  
 418 *quadrature points in all the cells, which, particularly for multi-dimensional velocity*  
 419 *domain, results in a memory intensive algorithm [7].*

420 **3.3 Properties of the evolution scheme** The entropy-minimization problem  
 421 in (2.19) ensures that our moment approximation conserves mass, moment and energy.  
 422 In addition to being conservative, the following discussion establishes that our space-  
 423 time discrete moment approximation (i) under a CFL-type condition, results in a  
 424 feasible optimization problem; and (ii) is L2 stable in the sense that the L2-energy  
 425  $\sum_{i=1}^{N_x} \|\langle P_M f_i^k \rangle_N\|_{l^2}^2$  has an upper-bound that depends solely on the initial data  $f_0$   
 426 and the boundary data  $f_{in}$ .

427 We start with making the following assumptions on the initial and the boundary  
 428 data. We assume that the first  $M$ -moments of  $f_0$  and  $f_{in}$  belong to the realizability  
 429 set  $R$  defined in (2.10) i.e.,

$$430 \quad (3.10) \quad \langle P_M f_{in}(x, t, \cdot) \rangle_N \in R, \quad \langle P_M f_0(x, \cdot) \rangle_N \in R, \quad \forall (x, t) \in \Omega \times D.$$

431 The above assumption will be helpful in establishing the feasibility of the optimization  
 432 problem in the optimization step. For the boundary data, we also assume that

$$433 \quad (3.11) \quad |f_{in}(\cdot, t, \cdot)|_{\partial\Omega, N} < \infty, \quad \forall t \in D,$$

where  $|f_{in}(\cdot, t, \cdot)|_{\partial\Omega, N} := \sum_{\xi_i \cdot n(x) \leq 0} \oint_{\partial\Omega} |\xi_i \cdot n(x)| f_{in}(x, t, \xi_i)^2 \omega_i ds$ .

434 Above, the unit vector  $n(x)$  is as given in (2.12), and  $\{\xi_i\}$  and  $\{\omega_i\}_i$  are the abscissas  
 435 and the weights of the quadrature points, respectively. Note that the assumption  
 436 on  $|f_{in}(\cdot, t, \cdot)|_{\partial\Omega, N}$  is a discrete-in-velocity analogue of a standard assumption that  
 437  $f_{in}(\cdot, t, \cdot) \in L^2(\partial\Omega_-, |\xi \cdot n(x)|)$ —see [40] for further details. Here,  $L^2(\partial\Omega_-, |\xi \cdot n(x)|)$   
 438 represents a  $L^2$  space over  $\partial\Omega_-$  with the Lebesgue measure  $|\xi \cdot n(x)|$ , and the set  
 439  $\partial\Omega_-$  contains all the incoming velocities and is as defined in (2.12). Intuitively, the  
 440 above assumption states that the total L2-energy flux associated with  $f_{in}$  should be  
 441 bounded. We insist that the above assumptions are valid for most applications of  
 442 practical relevance.

443 **3.4 Feasibility of the optimization problem** We show that under a CFL-  
 444 condition, the moments resulting from the collision step and the transport step belong  
 445 to the realizability set  $R$  given in (2.10) i.e., both the steps are realizability preserving.  
 446 The feasibility of the optimization problem then follows from Lemma 2.1. The details  
 447 are as follows.

448 Our result is a straightforward extension of the proof for the realizability preserv-  
 449 ing space-time discretization of radiative transport equations considered in [6]. Using  
 450 the definition of  $R$  given in (2.10), we find

$$451 \quad (3.12) \quad a_1 \lambda_1 + a_2 \lambda_2 \in R, \quad \forall a_1, a_2 \geq 0, \quad \lambda_1, \lambda_2 \in R.$$

453 We consider the collision step given in (3.7). Suppose that  $\langle P_M f_i^k \rangle \in R$ , which  
 454 implies that entropy-minimization step is well-posed (see [22]) and that  $\langle P_M f_{\mathcal{M},i}^k \rangle \in$   
 455  $R$ . Then, the above relation implies that for any  $\Delta t, \tau(x_i, t_k) > 0$ , the collision step  
 456 is realizability preserving i.e., for all  $i \in \{1, \dots, N_x\}$ , we have  $\langle P_M f_i^{k*} \rangle \in R$ .

457 We show that under a CFL-condition, the transport step in (3.8) is also realiz-  
 458 ability preserving. Replacing the numerical flux function from (3.9) in the transport  
 459 step given in (3.8) and re-arranging a few terms provides

$$(3.13) \quad \begin{aligned} \langle P_M f_i^{k+1} \rangle_N &= AL(1 - \Lambda|\Xi|)W(f_i^{k*}) \\ &+ \frac{\Lambda}{2}AL(|\Xi| - \Xi)W(f_{i+1}^{k*}) + \frac{\Lambda}{2}AL(|\Xi| + \Xi)W(f_{i-1}^{k*}). \end{aligned}$$

461 where  $\Lambda := \frac{\Delta t}{\Delta x}$ . For all  $i \in \{1, \dots, N_x\}$ , due to the positivity constraints in the  
 462 optimization problem (2.7), we have  $W(f_i^{k*}) > 0$ , which, for  $\Lambda > 0$ , implies that the  
 463 underlined terms are in  $R$ . To ensure that the first term on the right is in  $R$ , we  
 464 choose

$$(3.14) \quad 0 < \Lambda \leq \min\{|\xi_{\max}^{-1}|, |\xi_{\min}^{-1}|\}.$$

467 The above range of  $\Lambda$ , the relation in (3.12) and the assumption on the initial and  
 468 the boundary data (3.10) provides  $\langle P_M f_i^{k+1} \rangle_N \in R$ . We collect our findings in the  
 469 result below.

470 **LEMMA 3.1.** *Consider the evolution scheme outlined in Subsection 3.2 and de-*  
 471 *fine  $\Lambda = \Delta t / \Delta x$ . Assume that the initial and the boundary data satisfies (3.10),*  
 472 *then the quadratic optimization problem in the evolution scheme is feasible if  $\Lambda \in$*   
 473  *$(0, \min\{|\xi_{\max}^{-1}|, |\xi_{\min}^{-1}|\})$ .*

474 **3.5 L2 stability of the scheme** Define the total L2-energy at  $t = t_{k+1}$  as

$$(3.15) \quad \mathcal{E}_{k+1} := \sum_{i=1}^{N_x} \|\langle P_M f_i^{k+1} \rangle_N\|_{l^2}^2.$$

477 We establish that  $\mathcal{E}_{k+1}$  is bounded by the L2-energy of the previous time-step  $\mathcal{E}_k$  and  
 478  $|f_{in}(\cdot, t_k, \cdot)|_{\partial\Omega, N}$ . Recursion then implies that  $\mathcal{E}_{k+1}$  is bounded solely by the initial  
 479 and the boundary data.

For convenience, we define a few objects. For a vector  $z \in \mathbb{R}^N$ , with  $\|z\|_L$  we represent the norm

$$\|z\|_L := \sqrt{z^T L z}.$$

480 Interpreting  $z$  as a vector that contains the value of a function  $g : \Omega_\xi \rightarrow \mathbb{R}$  at the quad-  
 481 rature points and recalling that  $L$  is a diagonal matrix with the quadrature weights  
 482 on its diagonal, we conclude that  $\|z\|_L$  represent an approximation to  $\|g\|_{L^2(\Omega_\xi)}$ . We  
 483 bound the  $l^2$ -norm of a moment vector  $\lambda = ALz$  as

$$(3.16) \quad \|\lambda\|_{l^2} \geq \sigma_{\min}(A\sqrt{L})\|z\|_L, \quad \|\lambda\|_{l^2} \leq \sigma_{\max}(A\sqrt{L})\|z\|_L,$$

484 where  $\sigma_{\min/\max}(A\sqrt{L})$  represent the minimum/maximum singular value of the matrix  
 485  $A\sqrt{L}$ . We will use the above two bounds to convert stability results for the DVM to  
 486 stability results for the moment approximation.

489 **3.5.1 Collision step** We start with the collision step given in (3.6). Applying  
 490 triangle's inequality to the collision step we find

$$491 \quad (3.17) \quad \mathcal{E}_{k^*} \leq \frac{2}{(1 + \Delta t/\tau)^2} \mathcal{E}_k + 2 \left( \frac{\Delta t/\tau}{1 + \Delta t/\tau} \right)^2 \sum_{i=1}^{N_x} \underbrace{\|\langle P_M f_{\mathcal{M},i}^k \rangle_N\|_{l^2}^2}_{\leq \sigma_{\max}(A\sqrt{L})^2 \|W(f_{\mathcal{M},i}^k)\|_L^2} .$$

492 The bound on the right hand side follows from the inequalities in (3.16). From page-92  
 493 of [23] we know that the solution to the entropy-minimization problem (2.16) satisfies

$$494 \quad (3.18) \quad \|W(f_{\mathcal{M},i}^k)\|_L^2 \leq N^3 \exp(2Nt_k).$$

496 The above relation and the bound on  $\mathcal{E}_{k^*}$  given in (3.17) provides

$$497 \quad (3.19) \quad \mathcal{E}_{k^*} \leq \frac{2}{(1 + \Delta t/\tau)^2} \mathcal{E}_k + 2 \left( \frac{\Delta t/\tau}{1 + \Delta t/\tau} \right)^2 N_x \sigma_{\max}(A\sqrt{L})^2 N^3 \exp(2Nt_k).$$

499 **3.5.2 Transport step** With the following three steps, we establish the stability  
 500 of the transport step given in (3.8). (i) We recover a DVM underlying the transport  
 501 step in (3.8). (ii) Using stability properties of an upwind scheme, we establish the  
 502 stability of the DVM. (iii) Finally, relating the discrete velocity solution to the moment  
 503 solution, we establish the stability of the moment scheme. The details of these three  
 504 steps is as follows.

505 We consider the reformulated transport step given in (3.13). Let  $\mathcal{N}(AL)$  represent  
 506 the null-space of the matrix  $AL$ , where  $A$  and  $L$  are as given in (2.8) and (2.9),  
 507 respectively. Then, the transport step provides

$$508 \quad (3.20) \quad \begin{aligned} W(f_i^{k+1}) &= (1 - \Lambda|\Xi|)W(f_i^{k^*}) \\ &+ \frac{\Lambda}{2}(|\Xi| - \Xi)W(f_{i+1}^{k^*}) + \frac{\Lambda}{2}(|\Xi| + \Xi)W(f_{i-1}^{k^*}) + v, \end{aligned}$$

509 where  $v$  belongs to  $\mathcal{N}(AL)$ . Since the moments at time step  $t_{k+1}$ —given as  $ALW(f_i^{k+1})$ —  
 510 are invariant under the choice of  $v$ , we choose  $v = 0$ . This makes the above evolution  
 511 equation a space-time discretization of a system of decoupled linear advection equa-  
 512 tions given as  $\partial_t W(f) + \Xi \partial_x W(f) = 0$ . The discretization uses an explicit Euler and  
 513 an upwind FV scheme to discretize the space and the time domain, respectively. From  
 514 Example-7.2 of [33] we know that such a discretization is L2-stable under the CFL  
 515 condition

$$516 \quad (3.21) \quad 0 < \Lambda \leq \min\{|\xi_{\max}^{-1}|, |\xi_{\min}^{-1}|\}/2.$$

518 This provides

$$519 \quad (3.22) \quad \sum_{i=1}^{N_x} \|W(f_i^{k+1})\|_L^2 \leq \sum_{i=1}^{N_x} \|W(f_i^{k^*})\|_L^2 + |f_{in}(\cdot, t_k, \cdot)|_{\partial\Omega, N}^2.$$

521 Above,  $|\cdot|_{\partial\Omega, N}$  is as defined in (3.11). Using the bounds in (3.16), we express the  
 522 above bound in terms of moments to find

$$523 \quad (3.23) \quad \mathcal{E}_{k+1} \leq \kappa(A\sqrt{L})^2 \mathcal{E}_{k^*} + \sigma_{\max}(A\sqrt{L})^2 |f_{in}(\cdot, t_k, \cdot)|_{\partial\Omega, N}^2.$$

525 Above,  $\kappa(A\sqrt{L})$  represents the condition number of the matrix  $A\sqrt{L}$ . We collect our  
 526 stability estimate in the result below.

527 **THEOREM 3.2.** Consider the evolution scheme given in [Subsection 3.2](#) and let  $\mathcal{E}_k$   
 528 be the L2-energy defined in (5.5). Assume that the boundary data satisfies (3.10)  
 529 and that the ratio  $\Lambda = \Delta t/\Delta x$  satisfies  $\Lambda \in (0, \min\{|\xi_{\max}^{-1}|, |\xi_{\min}^{-1}|\}/2]$ . Then,  $\mathcal{E}_{k+1}$  is  
 530 bounded as

$$531 \quad (3.24) \quad \mathcal{E}_{k+1} \leq \mathcal{B}_k + \mathcal{B}_{\mathcal{M}} + \mathcal{B}_{in}$$

532 where

$$533 \quad (3.25) \quad \begin{aligned} \mathcal{B}_k &:= \kappa(A\sqrt{L})^2 \frac{2}{(1 + \Delta t/\tau)^2} \mathcal{E}_k, \\ \mathcal{B}_{\mathcal{M}} &:= 2\kappa(A\sqrt{L})^2 \sigma_{\max}(A\sqrt{L})^2 \left( \frac{\Delta t/\tau}{1 + \Delta t/\tau} \right)^2 N_x N^3 \exp(2Nt_k), \\ \mathcal{B}_{in} &:= \sigma_{\max}(A\sqrt{L})^2 |f_{in}(\cdot, t_k, \cdot)|_{\partial\Omega, N}^2. \end{aligned}$$

534 We make the following remarks related to the above theorem.

- 535 1. The terms  $\mathcal{B}_k$ ,  $\mathcal{B}_{\mathcal{M}}$  and  $\mathcal{B}_{in}$  appearing in (3.24) represent the contribution  
 536 from the previous time step, the discrete Maxwell-Boltzmann distribution  
 537 function and the boundary data, respectively, into bound for the L2-energy  
 538 at time  $t_{k+1}$ . Note that out of all these three terms, only  $\mathcal{B}_k$  depends upon  
 539 the solution of the previous time-step.
- 540 2. For the limit  $\tau \rightarrow 0$ , at least formally, the BE results in the Euler equations  
 541 [13]. Under this limit, the bound in (3.24) is robust, which is a result of  
 542 performing the collision step implicitly.
- 543 3. The DVM corresponding to the transport step given in (3.20) is a space-  
 544 time discretization of a linear hyperbolic PDE. As a result, the L2-bound  
 545 for the transport step (given in (3.23)) is linear in time. In contrast, since  
 546 the collision operator is non-linear, the collision step is non-linear. One can  
 547 attribute this non-linearity to the exponential-in-time growth in  $\mathcal{B}_{\mathcal{M}}$ .
- 548 4. For a fixed truncated velocity domain  $\Omega_\xi$ , consider the limit  $N, M \rightarrow \infty$  with  
 549  $N > M$ . Under this limit, the bound on  $\mathcal{E}_{k+1}$  is not robust because—at least  
 550 heuristically—both  $\kappa(A\sqrt{L})$  and  $\sigma_{\max}(A\sqrt{L})$  are almost independent of  $N$   
 551 and grow polynomially with  $M$ . To derive bounds that are independent of  
 552  $\kappa(A\sqrt{L})$  and  $\sigma_{\max}(A\sqrt{L})$ , one should directly consider the moment approxi-  
 553 mation without accessing the underlying DVM. As yet, it is unclear how to  
 554 proceed with such a technique.
- 555 5. Nowhere in the proof of the above theorem we used the fact that we minimize  
 556 the L2-norm in the moment-closure problem given in (2.7). Therefore, the  
 557 bound on  $\mathcal{E}_{k+1}$  holds for any other objective functional and specifically for  
 558 the minimum-entropy closure considered in [16, 30].

559 **3.6 Computational costs** We study the cost of evolution scheme outlined in  
 560 [Subsection 3.2](#). We consider the cost of a single time-step performed in a single spatial  
 561 cell.

- 562 1. *Entropy-minimization step:* We use Newton iteration to solve the entropy-  
 563 minimization problem where we compute and invert a Hessian  $H(x, t)$  given as  
 564  
 565

$$566 \quad (3.26) \quad (H(x, t))_{kl} := \sum_i (P_{\text{cons}}(\xi_i))_k (P_{\text{cons}}(\xi_i))_l \exp(P_{\text{cons}} \cdot \alpha(x, t)) \omega_i,$$

567

where  $\alpha(x, t)$  are the Lagrange multipliers in  $\mathbb{R}^3$ . Computing the Hessian is an  $\mathcal{O}(N)$  operation. As a stopping criterion to the Newton solver, we consider a user-defined tolerance of TOL in the moment constraints. Suppose we need  $m_{\text{TOL}}$  Newton iterations to reach this tolerance then, the total cost of entropy-minimization is given as

$$C_{\text{entropy}} = \mathcal{O}(Nm_{\text{TOL}}).$$

568

In all our numerical examples, we choose  $\text{TOL} = 10^{-8}$ .

2. *Collision step:* Computing the  $M$ -moments of the discrete Maxwell-Boltzmann pdf is an  $\mathcal{O}(NM)$  operation and updating the moments in the collision step is an  $\mathcal{O}(M)$  operation. Thus, the total cost of the collision step is given as

$$C_{\text{col}} = \mathcal{O}(MN).$$

569

3. *Optimization step:* We use the `quadprog` routine from matlab to solve the optimization problem in (2.7) and we use the default interior-point-convex solver with all the parameters set to their default values. Usually, it is difficult to estimate the complexity of this algorithm but a crude estimate gives [42]

570

571

572

$$(3.27) \quad C_{\text{opt}} = \mathcal{O}(N^3).$$

573

574

4. *Transport step:* Flux computation is an  $\mathcal{O}(MN)$  operation and the time update of the moments is an  $\mathcal{O}(M)$  operation. Thus the cost of the transport step is

$$C_{\text{tran}} = \mathcal{O}(MN).$$

Summing up the above costs, the total cost of our evolution scheme is given as

$$C_{\text{total}} = \mathcal{O}(Nm_{\text{TOL}}) + \mathcal{O}(MN) + \mathcal{O}(N^3).$$

575

**REMARK 7** (Efficiency of the optimization step). *For  $N > M$  (the values of  $N$  that interest us, see Remark 3) and a sufficiently small  $m_{\text{TOL}}$ , solving the quadratic optimization problem is the most expensive part of the algorithm. A possible way to overcome this high cost is to train an auto-encoder/gaussian-regression to replace the quadratic optimization problem [17, 25]. We plan to consider this direction in the future.*

576

577

578

579

580

581

#### 4 Extension to multi-dimensions

582

Maintaining consistency with our numerical experiments, we propose an extension of our method to two-dimensional planar flows. An extension to three-dimensional problems is similar and is not discussed for brevity. For 2D problems, we reduce the storage requirements by solving for the reduced pdfs  $h_1$  and  $h_2$  given as [41]

583

584

585

586

$$(4.1) \quad \begin{aligned} h_1(x, t, \xi_1, \xi_2) &:= \int_{\mathbb{R}} f(x, t, \xi_1, \xi_2, \xi_3) d\xi_3, \\ h_2(x, t, \xi_1, \xi_2) &:= \int_{\mathbb{R}} \xi_3^2 f(x, t, \xi_1, \xi_2, \xi_3) d\xi_3. \end{aligned}$$

587

In the coming discussion,  $\xi$  will represent a velocity vector in  $\mathbb{R}^2$  and with  $\langle g \rangle$  we will represent the integral of a function  $\xi \mapsto g(\xi)$  over  $\mathbb{R}^2$ . To derive the governing

588

589 equation for  $h_1$  and  $h_2$ , we multiply the BE given in (1.1) by 1 and  $\xi_3^2$  and integrate  
590 over  $\mathbb{R}$  with respect to  $\xi_3$  to find

$$591 \quad (4.2) \quad \partial_t h_i + \xi_1 \partial_{x_1} h_i + \xi_2 \partial_{x_2} h_i = \frac{1}{\tau} (h_{i,\mathcal{M}} - h_i).$$

593 Above,  $h_{i,\mathcal{M}}$  represents the reduced Maxwell-Boltzmann pdf and is given as

$$594 \quad (4.3) \quad h_{1,\mathcal{M}} = \frac{\rho}{2\pi\theta} \exp\left(-\frac{|\xi - v|^2}{2\theta}\right), \quad h_{2,\mathcal{M}} = \frac{\rho}{2\pi} \exp\left(-\frac{|\xi - v|^2}{2\theta}\right),$$

596 where,  $|\cdot|$  is the Euclidian norm of a vector. Note that the mass  $\rho$ , the momentum  
597  $\rho v$  and the temperature  $\theta$  can be recovered from  $h_1$  and  $h_2$  via

$$598 \quad (4.4) \quad \rho = \langle h_1 \rangle, \quad \rho v = \langle \xi h_1 \rangle, \quad \rho\theta = \frac{1}{3} (\langle |\xi|^2 h_1 \rangle - \rho|v|^2 + \langle h_2 \rangle).$$

599 **4.1 Moment equations** The moment approximation we discuss below is the  
600 same for both  $h_1$  and  $h_2$ . Therefore, for the simplicity of notation, we present our  
601 approximation for some representative  $h$ . Similar to the 1D case, we truncate the  
602 velocity domain to  $\mathbb{R}^2 \supset \Omega_\xi = [\xi_{1,\min}, \xi_{1,\max}] \times [\xi_{2,\min}, \xi_{2,\max}]$ . To compute  $\xi_{i,\max/\min}$ ,  
603 we adopt the same methodology as that outlined in Subsection 2.4. We consider ten-  
604 sorized  $N \times N$  Gauss-Legendre quadrature points inside  $\Omega_\xi$ . Using these quadrature  
605 points, we approximate  $\langle \cdot \rangle$  by  $\langle \cdot \rangle_{N,N}$ .

606 To derive a governing equation for the moments of  $h$ , we first define a polynomial  
607 in  $\xi$ . With  $\beta_M := (\beta_1^M, \beta_2^M) \in \mathbb{R}^2$  we represent a multi-index with each entry being  
608 a natural number and the  $l^1$ -norm of  $\beta_M$  being equal to  $M$ . Using  $\beta_M$ , we define  
609 a  $M$ -th order polynomial in  $\xi$  via  $p_{\beta_M} = \xi_1^{\beta_1^M} \xi_2^{\beta_2^M}$ . Note that for a given  $M$ ,  $\beta_M$  is  
610 non-unique—for  $M = 1$ ,  $\beta_M$  could either be  $(0, 1)$  or  $(1, 0)$ . In a vector  $P_M(\xi)$ , we  
611 collect all the polynomials  $p_{\beta_M}$  upto order  $M - 1$ . For completeness, we present the  
612 entries in  $P_M(\xi)$  for  $M = 3$  and  $M = 5$ .

$$613 \quad (4.5) \quad \begin{aligned} \text{M=3: } P_M(\xi) &= (1, \xi_1, \xi_2, \xi_1^2, \xi_1 \xi_2, \xi_2^2)^T; \\ \text{M=5: } P_M(\xi) &= (1, \xi_1, \xi_2, \xi_1^2, \xi_1 \xi_2, \xi_2^2, \xi_1^3, \\ &\quad \xi_1^2 \xi_2, \xi_1 \xi_2^2, \xi_2^3, \xi_1^4, \xi_1^3 \xi_2, \xi_1^2 \xi_2^2, \xi_1 \xi_2^3, \xi_2^4)^T. \end{aligned}$$

614 Note that for  $M = 3$  and  $M = 5$ ,  $P_M(\xi)$  contains 6 and 15 entries, respectively.

615 For some  $M \in \mathbb{N}$ , we approximate  $h$  by  $h_M$  where we compute  $h_M$  (more precisely  
616  $W(h_M)$ ) using the L2-minimization problem given in (2.7). To evolve the moments of  
617  $h_M$ , we use a multi-dimensional version of the moment system given in (2.18), which  
618 reads

$$619 \quad (4.6) \quad \begin{aligned} \partial_t \langle P_M h_M \rangle_{N,N} + \partial_{x_1} \langle P_M \xi_1 h_M \rangle_{N,N} + \partial_{x_2} \langle P_M \xi_2 h_M \rangle_{N,N} \\ = \frac{1}{\tau} (\langle P_M h_{\mathcal{M},N} \rangle_{N,N} - \langle P_M h_M \rangle_{N,N}) \text{ on } \Omega \times D, \\ \langle P_M h_M(t=0) \rangle_{N,N} = \langle P_M h_0 \rangle_{N,N} \text{ on } \Omega. \end{aligned}$$

620 Above,  $h_{\mathcal{M},N}$  is a discretization of the Maxwell-Boltzmann pdf that results from  
621 solving a multi-dimensional version of the optimization problem given in (2.16)—see  
622 [22] for an explicit form of this optimization problem. The treatment of boundary  
623 conditions is the same as that for the 1D case and is not discussed for brevity.



624 **4.2 Space-time discretization** For simplicity, we consider a square spatial  
 625 domain  $\Omega = [x_{1,\min}, x_{1,\max}] \times [x_{2,\min}, x_{2,\max}]$ . We discretize  $\Omega$  with  $N_x$  number of  
 626 uniform elements in each spatial dimension and with  $\Delta x$  we represent the grid spacing.  
 627 With some additional technical details, it is straightforward to extend our framework  
 628 to curved domain discretized with unstructured meshes. For simplicity, we consider  
 629 a fixed time-step of size  $\Delta t$ .

630 We index a spatial cell with  $(i, j)$  where  $i, j \in \{1, \dots, N_x\}$ . With  $\langle P_M h_{i,j}^k \rangle_{N,N}$   
 631 we represent a FV approximation to  $\langle P_M h_M(x, t_k, \cdot) \rangle_{N,N}$  in the cell  $\mathcal{I}_{i,j}$ . Given  
 632  $\langle P_M h_{i,j}^k \rangle_{N,N}$ , we want to compute the FV approximation at the next time instance.  
 633 To this end, we follow the same four steps as those outlined for the 1D-case in [Sub-](#)  
 634 [section 3.2](#). The entropy-minimization step, the collision step and the optimization  
 635 step are very similar to the 1D case and, for brevity, we do not repeat them here. The  
 636 transport step is slightly different and is given as

$$\begin{aligned}
 \frac{\langle P_M f_{i,j}^{k+1} \rangle_{N,N} - \langle P_M f_{i,j}^{k,*} \rangle_{N,N}}{\Delta t} &= -\frac{1}{\Delta x} \left( \mathcal{F}_1(W(f_{i+1,j}^{k,*}), W(f_{i,j}^{k,*})) \right. \\
 &\quad \left. - \mathcal{F}(W(f_{i,j}^{k,*}), W(f_{i-1,j}^{k,*})) \right) \\
 &\quad - \frac{1}{\Delta x} \left( \mathcal{F}_2(W(f_{i,j+1}^{k,*}), W(f_{i,j}^{k,*})) \right. \\
 &\quad \left. - \mathcal{F}_2(W(f_{i,j}^{k,*}), W(f_{i,j-1}^{k,*})) \right).
 \end{aligned}$$

637 (4.7)

638 Above,  $\{W(f_{i,j}^{k,*})\}_{i,j}$  results from the optimization step and  $\mathcal{F}_1(W_1, W_2)$  and  $\mathcal{F}_2(W_1, W_2)$   
 639 are the numerical fluxes given as

$$\mathcal{F}_i(W_1, W_2) := \frac{1}{2} (AL(\Xi_i - |\Xi_i|)W_1 + AL(\Xi_i + |\Xi_i|)W_2).$$

640 (4.8)  
 641

642 Above,  $A$  and  $L$  are multi-dimensional versions of the matrices given in [\(2.8\)](#) and  $\Xi_i$   
 643 is a diagonal matrix with all the  $i$ -th components of the quadrature point's locations  
 644 at its diagonal.

645 Assuming that the initial and the boundary data satisfies [\(3.10\)](#), one can show that  
 646 the space-time discretization results in a feasible optimization if the ratio  $\Lambda = \Delta t / \Delta x$   
 647 satisfies

$$0 < \Lambda \leq \frac{1}{2} \min_i \{ \min \{ |\xi_{i,\max}^{-1}|, |\xi_{i,\min}^{-1}| \} \}.$$

648 (4.9)  
 649

650 Similarly, one can show that the space-time discretization is L2-stable if  $\Lambda$  satisfies

$$0 < \Lambda \leq \frac{1}{4} \min_i \{ \min \{ |\xi_{i,\max}^{-1}|, |\xi_{i,\min}^{-1}| \} \}.$$

651 (4.10)  
 652

653 A proof of the above two results uses the exact same technique as that for the 1D  
 654 case and is not repeated for brevity.

655 **5 Numerical Results** For simplicity, we non-dimensionalize the BE and all  
 656 the macroscopic quantities with appropriate powers of some reference density  $\rho_0$ ,  
 657 temperature  $\theta_0$  and length scale  $l$ . This introduces the Knudsen number  $Kn$ , the  
 658 inverse of which scales the collision operator  $Q(f)$ , and reads  $Kn := \tau_0 / (\sqrt{\theta_0} l)$ —we  
 659 refer to [\[32\]](#) for the details of non-dimensionalization. In the definition of the collision  
 660 frequency  $\tau(x, t)^{-1}$  given in [\(2.14\)](#), we choose  $C = 1$  and  $\omega = 1$ . Our choice of  $C$  and

661  $\omega$  does not necessarily corresponds to a physical system and is made for demonstration  
662 purposes.

663 We consider the following test cases.

664 1. **Test case-1** We consider the pdf

$$665 \quad (5.1) \quad f(\xi) = \frac{1}{\sqrt{2\pi\theta_0}} \exp\left(-\frac{(\xi - u_0)^2}{2\theta_0}\right) + \frac{1}{\sqrt{2\pi\theta_1}} \exp\left(-\frac{(\xi - u_1)^2}{2\theta_1}\right).$$

666

667 Given the first  $M$  moments of  $f$  and using the pos-L2-MOM, we approximate  
668 the  $M + 1$ -st moment of  $f$ . We study the error of this approximation with  
669 respect to the number of moments  $M$ . We choose  $\theta_0 = 3$ ,  $u_0 = -4$ ,  $\theta_1 = 4$   
670 and  $u_1 = 5$ , which ensures that  $f$  is far away from a Maxwell-Boltzmann  
671 distribution function in the Kullback–Leibler divergence sense.

672 2. **Test case-2** For a one-dimensional space-velocity domain, we consider the  
673 Sod’s shock tube problem from [35]. We set  $\Omega = [-2, 2]$  and  $D = [0, 0.3]$ .  
674 Recall that  $D$  is the time domain. As the initial data, we consider a gas at  
675 rest and at equilibrium. We initialize the temperature  $\theta$  with a constant value  
676 of one and we initialize density as

$$677 \quad (5.2) \quad \rho(x, t = 0) = \begin{cases} 7, & x \leq 0 \\ 1, & x > 0 \end{cases}.$$

678

679 As the boundary data  $f_{in}$ , we consider a Maxwell-Boltzmann pdf. At  $x =$   
680  $x_{\min}$  and for all  $t \in D$ , we set density to 7, velocity to 0 and temperature  
681 to 1. The velocity and the temperature at the right boundary remains the  
682 same but the density changes to 1. We consider two different values of the  
683 Knudsen number— $Kn = 0.1$  and  $Kn = 0.01$ .

684 3. **Test case-3** For a one-dimensional space-velocity domain, we consider the  
685 two-beam interaction experiment from [30]. The space-time domain  $\Omega \times D$   
686 remains the same as the previous test case. As the initial data, we consider  
687 a gas at equilibrium with a constant density and temperature of one. As the  
688 initial velocity, we consider

$$689 \quad (5.3) \quad v(x, t = 0) = \begin{cases} 1, & x \leq 0 \\ -1, & x > 0 \end{cases}.$$

690

691 As the boundary data  $f_{in}$ , we consider a Maxwell-Boltzmann pdf. At  $x =$   
692  $x_{\min}$  and for all  $t \in D$ , we set density to 1, velocity to 1 and temperature  
693 to 1. The density and the temperature at the right boundary remains the  
694 same but the velocity changes to  $-1$ . We consider two different values of the  
695 Knudsen number— $Kn = 0.1$  and  $Kn = 0.01$ .

696 4. **Test case-4** We consider a two-dimensional spatial domain and a planar flow  
697 regime. We choose  $\Omega = [0, 2] \times [0, 2]$  and  $D = [0, 0.2]$ . We consider a micro-  
698 bubble dispersion problem where we start with a fluid at equilibrium and at  
699 rest. We consider a constant temperature of one and consider a density given  
700 as

$$701 \quad (5.4) \quad \rho(x, t = 0) = \rho_0 + \exp(-|x - 1|^2 \times 10^2), \quad \forall x \in \Omega.$$

702

703 As the ground state density, we set  $\rho_0 = 1$ . As the boundary data  $f_{in}$ ,  
704 we consider a Maxwell-Boltzmann pdf with a density  $\rho_0$ , velocity zero and  
705 temperature one. We consider a Knudsen number of 0.1.

706 We emphasize that for this test case, it is crucial that the moment-closure  
 707 problem has a positive solution. Otherwise, the density can get negative  
 708 resulting in a breakdown of the solution algorithm. We refer to [27] for  
 709 a similar experiment involving the linearized BE and the Grad’s Hermite  
 710 expansion, which is not necessarily positive. There, the deviation in density  
 711 gets negative for small values of  $M$ . However, since the BE is linearized,  
 712 negative densities do not crash the solution algorithm.

713 **5.1 Test case-1** We truncate the velocity domain to  $\Omega_\xi = [-20, 20]$ . This  
 714 ensures that the support of  $f$  (upto machine precision) is contained inside  $\Omega_\xi$ . We  
 715 compute  $W(f_M)$  using the optimization problem given in (2.7).

716 **5.1.1 Error in the higher order moment** Recall that we used  $f_M$  to close  
 717 the moment system in (2.18) by approximating the  $M$ -th order moment of  $f$ . The  
 718 relative error of this approximation is given as

$$719 \quad (5.5) \quad \mathcal{E}(M) := \left| \frac{\langle \xi^M (f_M - f) \rangle_N}{\langle \xi^M f \rangle_N} \right|.$$

720

721 We study  $\mathcal{E}(M)$  for different values of  $M$ . We vary  $M$  from 3 to 22 in steps of one,  
 722 and we fix  $N$  at a sufficiently large value of 40.

723 As  $M$  increases,  $\mathcal{E}(M)$  appears to converge to zero, although not monotonically—  
 724 see Figure 1a. Note that this non-monotonic convergence is typical also for a Grad’s  
 725 moment approximation [11, 27, 36]. However, unlike the Grad’s moment approxima-  
 726 tion where the error convergences monotonically for either the even or the odd values  
 727 of  $M$ , the convergence behaviour of the pos-L2-MOM is rather random. For instance,  
 728 the error (slightly) increases from  $M = 5$  to  $M = 7$ . Similarly, the error (slightly)  
 729 increases from  $M = 15$  to  $M = 17$ . Nevertheless, for  $M \geq 16$ , the error appears to  
 730 converge monotonically.

731 **5.1.2 Error in approximating the pdf** For different values of  $M$ , Figure 1b  
 732 compares  $f$  to  $f_M$ . To extend the discrete values of  $f_M$  to  $\Omega_\xi$ , we perform a piecewise  
 733 linear interpolation between the quadrature points. For  $M = 3$ , pos-L2-MOM is  
 734 unable to capture the general shape of the function. Nevertheless, increasing the  
 735 value of  $M$  improves the results. Already for  $M = 5$ , we observe that  $f_M$  has two  
 736 distinct peaks and starts to capture the shape of the function. Increasing  $M$  from  
 737 5 to 7 does not show much of an improvement. However, increasing  $M$  from 7 to 9  
 738 improves the results significantly. The result for  $M = 9$  almost overlaps the exact  
 739 solution with little deviations. Let us mention that for all values of  $M$ ,  $f_M$  remains  
 740 positive.

741 For a comparison, we compute a DG approximation of  $f$ . We represent the DG  
 742 approximation by  $f_M^{DG}$  and compute it by projecting  $f$  (under the  $L^2(\Omega_\xi)$  inner-  
 743 product) onto the first  $M$  Legendre polynomials in  $\xi$ . For the different values of  $M$ ,  
 744 Figure 1c compares  $f$  to  $f_M^{DG}$ . Since a DG approximation does not penalize negativity  
 745 (see Remark 1), for all values of  $M$ ,  $f_M^{DG}$  is negative for some part of the velocity  
 746 domain. Furthermore, only for  $M \geq 11$ , the DG approximation starts to capture  
 747 the general shape of the function. Compare this to  $f_M$ , which, already for  $M = 5$ ,  
 748 accurately represents the shape of the function.

749 The superior accuracy of  $f_M$ —as compared to  $f_M^{DG}$ —in approximating  $f$  is clearly  
 750 visible in Figure 1d, which compares the relative L2-error in approximating  $f$ . The  
 751 difference between the error values becomes larger as the value of  $M$  increases. For the  
 752 largest value of  $M$  equals 22, the relative L2-error resulting from the approximation  $f_M$

753 is  $8 \times 10^{-4}$ , which is  $\approx 10^{-2}$  times smaller than that resulting from the approximation  
 754  $f_M^{DG}$ .

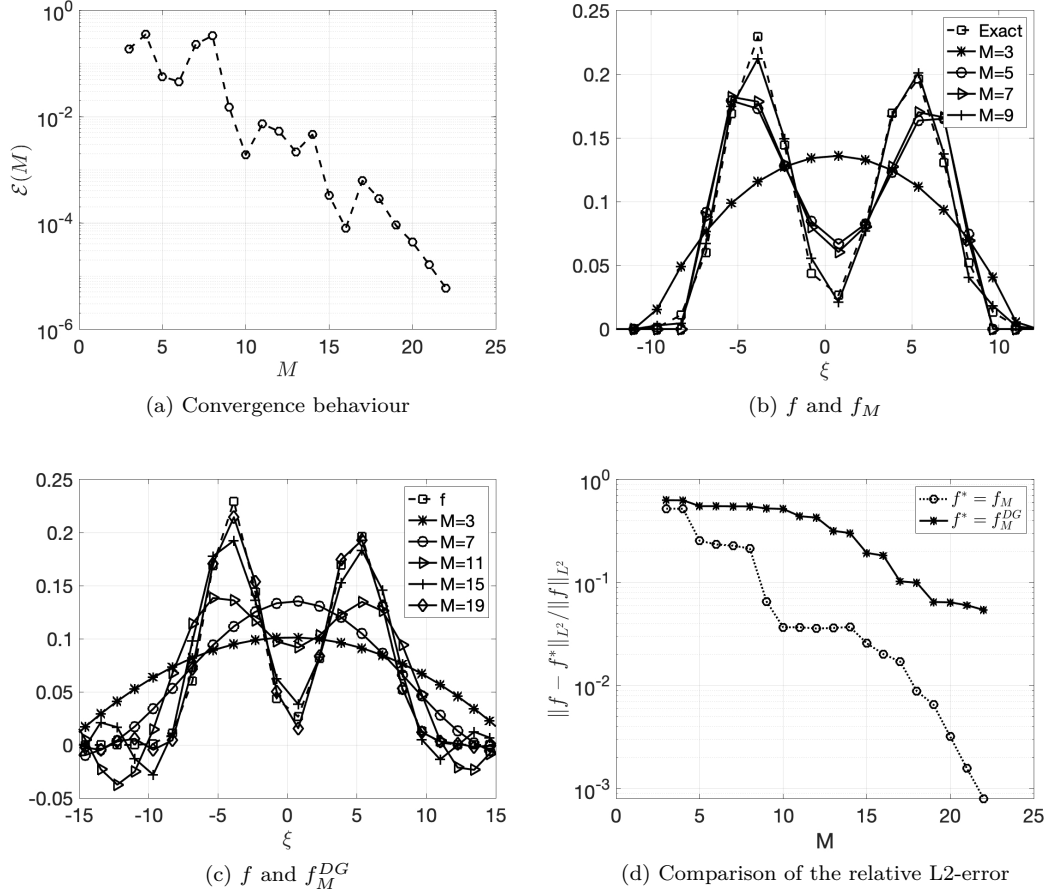


Fig. 1: Results for test case-1. (a) and (d) y-axis is on a log-scale.

755

## 5.2 Test case-2

756

757 **5.2.1 Reference solution** We compute the reference solution using a DVM  
 758 proposed in [22]. We consider an explicit Euler time-stepping scheme and a first-  
 759 order FV spatial discretization. We truncate the velocity domain to  $[-7, 7]$ , and  
 760 place  $N = 350$  velocity grid points inside the truncated velocity domain. As the  
 761 velocity grid points, we consider Gauss-Legendre quadrature nodes. We discretize  
 762 the space domain with  $N_x = 10^3$  uniform cells and consider a constant time-step  
 763 of  $\Delta t = 0.5 \times \Delta x / 7$ . To arrive at these discretization parameters, we performed a  
 764 convergence study that consisted of the following steps. (i) With the velocity and  
 765 the temperature field taken from the initial data, estimate  $\xi_{\max/\min}$  using the relation  
 766 in (2.20). For the present test case, this provides  $\xi_{\max} = 3.5$  and  $\xi_{\min} = -3.5$ . (ii)  
 767 Fix  $N_x$  at  $10^3$  and  $\Delta t$  to  $0.5 \times \Delta x / \xi_{\max}$ . (iii) Choose  $N = 50$  and increase it to  
 350 in steps of 50. (iv) Terminate the refinement as soon as the relative change in

768 mass, momentum and energy between two subsequent refinement cycles drops below  
 769 a tolerance of  $10^{-5}$ . (v) If the tolerance is not reached, increase  $\xi_{\max}$  by 0.5, decrease  
 770  $\xi_{\min}$  by 0.5 and repeat the process from step-(ii). Note that if the refinement cycle  
 771 does not terminate then one should increase the value of  $N_x$  and repeat the entire  
 772 process. For the all the test cases mentioned earlier, the value of  $N_x = 10^3$  was  
 773 sufficiently large to terminate the refinement cycle.

774 **5.2.2 Convergence study** We are interested in the relative L2 error in the  
 775 different macroscopic quantities that we define as

$$776 \quad (5.6) \quad \mathcal{E}_{cons}(M, N_x) := \frac{\| \langle P_{cons}(f_{M, N_x}(\cdot, t = T, \cdot) - f_{DVM}(\cdot, t = T, \cdot)) \rangle_N \|_{L^2(\Omega; \mathbb{R}^3)}}{\| \langle P_{cons} f_{DVM}(\cdot, t = T, \cdot) \rangle_N \|_{L^2(\Omega; \mathbb{R}^3)}}.$$

778 Above,  $P_{cons}$  and  $f_{M, N_x}$  are as defined in (2.13) and (3.4), respectively. We keep the  
 779 value of  $N$  fixed at 30.

780 We first consider  $\text{Kn} = 0.1$ . We increase  $M$  from 3 to 10 in steps of 1 and  $N_x$   
 781 from 200 to  $10^3$  in steps of 200. We choose  $\Delta t = 0.5 \times \Delta x / 7$ . Figure 2a shows  
 782 the error  $\mathcal{E}_{cons}(M, N_x)$  for the different values of  $M$  and  $N_x$ . Fixing  $N_x$  at a small  
 783 value—200 for instance—and increasing  $M$  does not reduce the error. This is be-  
 784 cause for small values of  $N_x$ , the error is dominated by the error in our space-time  
 785 discretization. Furthermore, for a small value of  $M$ , increasing  $N_x$  beyond a certain  
 786 limit does not decrease the error. On the other hand, choosing a large value of  $N_x$ —  
 787  $10^3$  for instance—and increasing  $M$ , or increasing both  $M$  and  $N_x$  simultaneously,  
 788 reduces the error. Note that similar to the previous test case, the error decay is not  
 789 monotonic. Our results suggest that to balance the accuracy with the computational  
 790 cost, an adaptive choice of  $M$  and an adaptive spatial grid is desirable. We plan to  
 791 develop such an adaptive framework in the future—see [2] for an adaptive moment  
 792 method. Let us also mention that at  $N_x = 10^3$  and  $M = 10$ , we attain a minimum  
 793 relative error of  $2.4 \times 10^{-2}$ . We find this error value acceptable, given that  $M = 10$   
 794 is less than 10% of the velocity grid points used in our reference DVM.

795 We now consider  $\text{Kn} = 0.01$ . We choose  $M$  and  $N_x$  as before. Figure 2a shows the  
 796 error  $\mathcal{E}_{cons}(M, N_x)$  for the different values of  $M$  and  $N_x$ . As compared to  $\text{Kn} = 0.1$ ,  
 797 the smaller values of  $M$  perform much better, which is in accordance with similar  
 798 studies conducted in the previous works [36]. For instance, consider the results for  
 799  $M = 4$  and  $N_x = 10^3$ . For  $\text{Kn} = 0.1$ , we find  $\mathcal{E}_{cons}(4, 10^3) = 1.3 \times 10^{-1}$ , whereas for  
 800  $\text{Kn} = 0.01$  we find  $\mathcal{E}_{cons}(4, 10^3) = 2.5 \times 10^{-2}$ , which is almost an order-of-magnitude  
 801 better than the result for  $\text{Kn} = 0.1$ .

802 Although the lower values of  $M$  perform better for  $\text{Kn} = 0.01$  than for  $\text{Kn} = 0.1$ ,  
 803 the minimum error attained is almost the same for both the Knudsen number—  
 804 for  $\text{Kn} = 0.01$  the minimum error is  $2.3 \times 10^{-3}$ , which is 0.95 times that of the  
 805 minimum error for  $\text{Kn} = 0.1$ . This is because for  $\text{Kn} = 0.01$ , the error at  $N_x = 10^3$  is  
 806 already dominated by the error in our spatial discretization and we see almost no error  
 807 reduction upon increasing  $M$  from 7 to 10. By increasing  $N_x$  from  $10^3$  to  $1.5 \times 10^3$ ,  
 808 we could remove this error stagnation and for  $M = 10$ , achieve an error of  $1.2 \times 10^{-3}$ .  
 809

810 **5.2.3 Sub-shocks** Shock speeds that are faster than the characteristic speeds  
 811 in a moment system result in sub-shocks—we refer to [34] for an exhaustive study  
 812 of sub-shocks for the Grad’s MOM. Similar to the Grad’s MOM, the pos-L2-MOM  
 813 shows sub-shocks-type structures—see the density profile shown in Figure 3. These  
 814 structures have a staircase-type shape, and increasing  $M$  from 3 to 5 has a smoothing

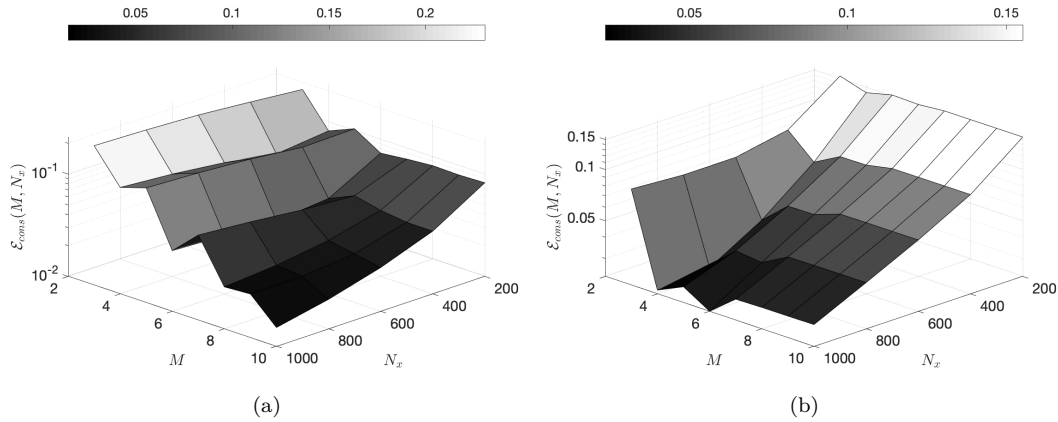


Fig. 2: Results for test case-2. Convergence of the relative error with  $N_x$  and  $M$ . Computations performed using the pos-L2-MOM. (a)  $Kn = 0.1$  and (b)  $Kn = 0.01$ . The z-axis on both the plots is on a log-scale.

815 effect that reduces the staircase effect. To conclude that these structures are indeed  
 816 sub-shocks, one needs to study the characteristic speeds of the moment system given  
 817 in (2.18). Note that these sub-shocks can be removed by introducing second-order  
 818 spatial derivatives in the moment equations via regularization—see the discussion on  
 819 the regularized-13 moment equations [39].

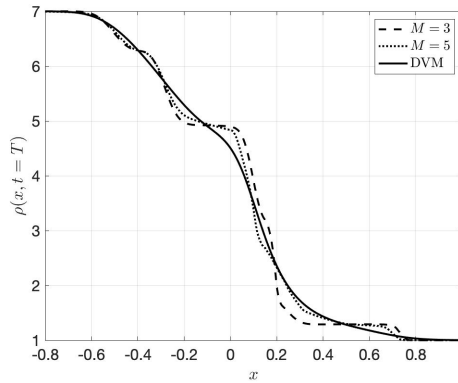


Fig. 3: Results for test case-2. Density profile for  $Kn = 0.1$  and at  $t = T$ . Computations performed with  $N_x = 10^3$  grid-cells.

820 **5.3 Test case-3** As before, we construct a reference solution using the DVM.  
 821 The convergence study discussed in Subsection 5.2.1 lead to  $N_x = 10^3$ ,  $\xi_{\max} = 5$ ,  
 822  $\xi_{\min} = -5$  and  $N = 350$ . For the pos-L2-MOM, we fix  $N = 30$  and  $N_x = 10^3$ ,  
 823 and study the results for two different values of  $M$ ,  $M = 5$  and  $M = 7$ . We choose  
 824  $\Delta t = 0.5\Delta x/\xi_{\max}$ . The convergence behaviour is similar to the previous test case and

825 not discussed for brevity.

826 For  $\text{Kn} = 0.1$  and  $M = 5$ , Figure 4a compares the density and the velocity  
 827 computed using the DVM and the pos-L2-MOM. The results for temperature are  
 828 similar and are not shown for brevity. The pos-L2-MOM performs well and results in  
 829 an error of  $\mathcal{E}_{cons}(5, 10^3) = 6.8 \times 10^{-2}$ . Furthermore, increasing the value of  $M$  from 5  
 830 to 7 improves the results and the error reduces to  $\mathcal{E}_{cons}(7, 10^3) = 2.5 \times 10^{-2}$ —Figure 4b  
 831 shows the result for  $M = 7$ . Reducing the Knudsen number to 0.01, improves the  
 832 results for both  $M = 5$  and  $M = 7$ —see Figure 4c and Figure 4d. For both the values  
 833 of  $M$ , we obtained an error of  $\mathcal{E}_{cons}(5/7, 10^3) = 9 \times 10^{-3}$ , which is approximately  
 834 1/3 of the error for  $\text{Kn} = 0.1$ . Note that similar to the previous test case, the error  
 835 for  $\text{Kn} = 0.01$  is dominated by the error in the space-time discretization. Therefore,  
 836 increasing  $M$  from 5 to 7 does not offer any improvement.

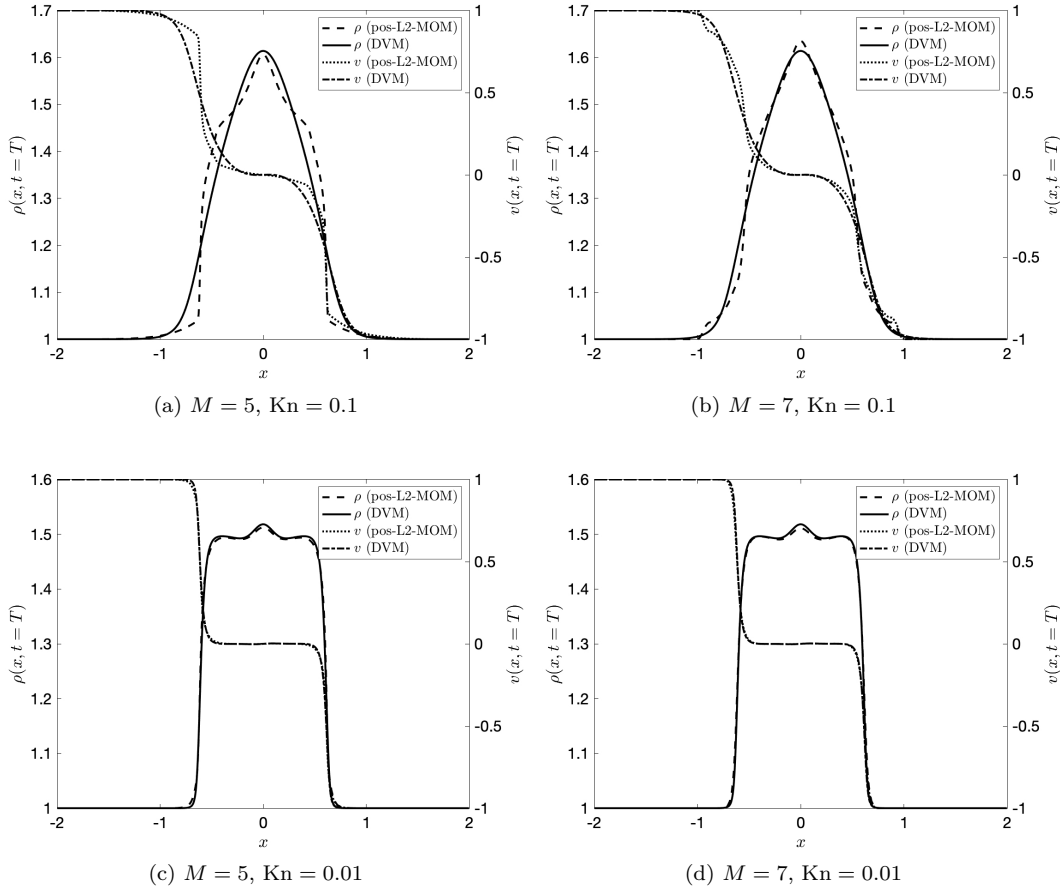


Fig. 4: Results for test case-3. Density and velocity profiles for different values of  $M$  and different Knudsen numbers. The left and the right y-axis is for density and velocity, respectively.

837 **5.4 Test case-4** Under the limited computational resources, we were unable  
 838 to compute a highly-refined reference solution in multi-dimensions. For this reason,  
 839 we refrain from performing a convergence study for the present test case. Rather,  
 840 we compare our moment method to a sufficiently refined DVM and showcase an  
 841 improvement in the moment solution by increasing  $M$ . For both the DVM and the  
 842 moment method, we consider tensorized Gauss-Legendre quadrature points with  $N =$   
 843 40 quadrature points in each direction. We place these quadrature points inside  
 844  $\Omega_\xi = [\xi_{\min}, \xi_{\max}] \times [\xi_{\min}, \xi_{\max}]$  with  $\xi_{\max} = 7$  and  $\xi_{\min} = -7$ . We discretize the  
 845 spatial domain with  $150 \times 150$  uniform elements with grid-size  $\Delta x = 1.3 \times 10^{-2}$ . We  
 846 consider a constant time-step of  $\Delta = \Delta x / (4 \times \xi_{\max})$ .

847 As time progresses, the density disperses into the spatial domain. This is made  
 848 clear by [Figure 5a](#) that shows the density profile at  $t = T$  computed using the DVM.  
 849 At the same time-instance, [Figure 5b](#) and [Figure 5c](#) show the density profile at  $t = T$   
 850 computed using the pos-L2-MOM with  $M = 3$  and  $M = 5$ , respectively. As expected,  
 851 both the density profiles are positive. Furthermore, the moment solution appears  
 852 to improve upon increasing the value of  $M$ . The improvement is quantified by the  
 853 decrease in the relative L2-error in density shown in [Table 1](#).

854 The dispersion of the micro-bubble triggers a flow velocity and a temperature  
 855 gradient. [Figure 6](#) compares the  $x_1$  velocity component and the temperature along a  
 856 cross-section of the spatial domain computed using the pos-L2-MOM and the DVM.  
 857 The results for the  $x_2$  velocity component are similar and are not shown for brevity.  
 858 As expected, similar to density, the results for both the velocity and the temperature  
 859 appear to improve as  $M$  is increased from 3 to 5, the relative L2-error shown in  
 860 [Table 1](#) indicates the same. We note that, as compared to the previous test cases, the  
 861 moment method performs better for the present test case. A possible reason for this  
 862 could be that our DVM solution is not as refined as for the previous test cases—the  
 863 previous test cases consider a 1D velocity grid of 350 points whereas the present test  
 864 case considers a tensorized grid of  $40 \times 40$  points.

$M$	$\rho$	$v_1$	$v_2$	$\theta$
3	$1.6 \times 10^{-3}$	$2 \times 10^{-1}$	$2.1 \times 10^{-1}$	$2.8 \times 10^{-3}$
5	$5.3 \times 10^{-4}$	$5 \times 10^{-2}$	$4.8 \times 10^{-2}$	$5.4 \times 10^{-4}$

Table 1: Results for test case-4. Relative  $L^2(\Omega)$ -error in different macroscopic quantities at  $t = T$  and  $Kn = 0.1$ .

865 **6 Conclusions** We proposed a positive moment method for the Boltzmann-  
 866 BGK equation based upon L2-minimization. We showed that on a space-time discrete  
 867 level both the feasibility of the minimization problem and the stability of the  
 868 moment approximation can be ensured via a CFL-type condition. Our proof of both  
 869 these properties relied on relating our moment method to a discrete-velocity-method.  
 870 Through an entropy-minimization based discretization of the collision operator, we  
 871 ensured that our moment approximation conserves mass, momentum and energy. We  
 872 also extended our method to a multi-dimensional space-velocity domain. With the  
 873 help of numerical experiments, we studied the accuracy of our method for both single  
 874 and multi-dimensional space-velocity domains. Our method performed well for a  
 875 broad range of problems involving strong shocks, beam interaction and micro-bubble  
 876 dispersion. Furthermore, it retained accuracy for a broad range of Knudsen numbers.



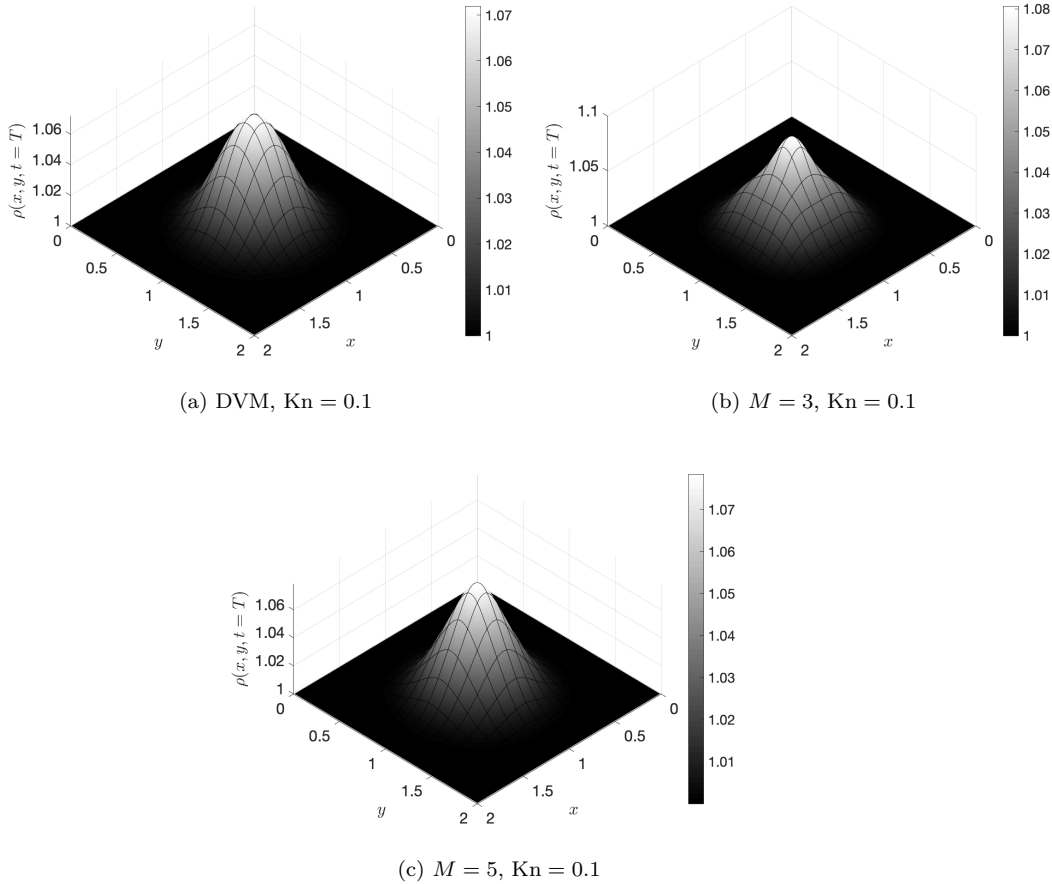


Fig. 5: Results for test case-4. Density profiles at  $t = T$ .

877

**References**

878

[1] M. R. A. Abdelmalik and E. H. van Brummelen. Moment closure approximations of the Boltzmann equation based on  $\phi$ -divergences. *Journal of Statistical Physics*, 164(1):77–104, Jul 2016.

879

880

[2] M. R. A. Abdelmalik and E. H. van Brummelen. Error estimation and adaptive moment hierarchies for goal-oriented approximations of the Boltzmann equation. *Computer Methods in Applied Mechanics and Engineering*, 325(Supplement C):219 – 239, 2017.

881

882

[3] A. Alekseenko and E. Josyula. Deterministic solution of the spatially homogeneous Boltzmann equation using discontinuous Galerkin discretizations in the velocity space. *Journal of Computational Physics*, 272:170 – 188, 2014.

883

884

[4] G. W. Alldredge, M. Frank, and C. D. Hauck. A regularized entropy-based moment method for kinetic equations. *SIAM Journal on Applied Mathematics*, 79(5):1627–1653, 2019.

885

886

[5] G. W. Alldredge, C. D. Hauck, D. P. O. Leary, and A. L. Tits. Adaptive change of basis in entropy-based moment closures for linear kinetic equations. *Journal*

887

888

889

890

891

892

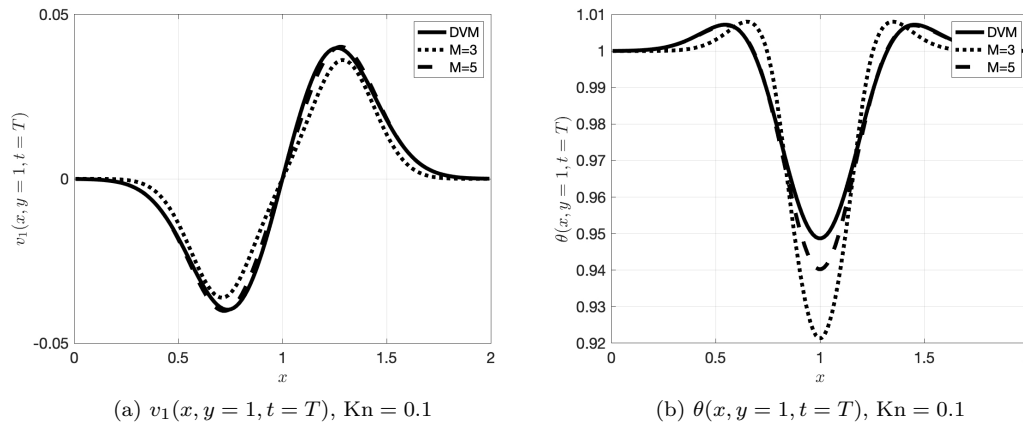


Fig. 6: Results for test case-4.  $v_1$  and  $\theta$  profiles.

- 893 of *Computational Physics*, 258:489 – 508, 2014.
- 894 [6] G. W. Alldredge, C. D. Hauck, and A. L. Tits. High-order entropy-based closures  
895 for linear transport in slab geometry ii: A computational study of the optimiza-  
896 tion problem. *SIAM Journal on Scientific Computing*, 34(4):B361–B391, 2012.
- 897 [7] C. Baranger, J. Claudel, N. Hérouard, and L. Mieussens. Locally refined discrete  
898 velocity grids for stationary rarefied flow simulations. *Journal of Computational*  
899 *Physics*, 257:572 – 593, 2014.
- 900 [8] N. Bohmer and M. Torrilhon. Entropic quadrature for moment approximations  
901 of the Boltzmann-BGK equation. *Journal of Computational Physics*, 401:108992,  
902 2020.
- 903 [9] S. Brull and L. Mieussens. Local discrete velocity grids for deterministic rarefied  
904 flow simulations. *Journal of Computational Physics*, 266:22 – 46, 2014.
- 905 [10] Z. Cai, Y. Fan, and L. Ying. An entropic Fourier method for the Boltzmann  
906 equation. *SIAM Journal on Scientific Computing*, 40(5):A2858–A2882, 2018.
- 907 [11] Z. Cai and M. Torrilhon. Numerical simulation of microflows using moment  
908 methods with linearized collision operator. *Journal of Scientific Computing*, 2017.
- 909 [12] C. Cercignani. *The Boltzmann Equation and Its Applications*. Springer, 67 edi-  
910 tion, 1988.
- 911 [13] S. Chapman, T. G. Cowling, and D. Burnett. *The mathematical theory of non-*  
912 *uniform gases: an account of the kinetic theory of viscosity, thermal conduction*  
913 *and diffusion in gases*. Cambridge university press, 1990.
- 914 [14] F. Filbet and S. Jin. A class of asymptotic-preserving schemes for kinetic equa-  
915 tions and related problems with stiff sources. *Journal of Computational Physics*,  
916 229(20):7625 – 7648, 2010.
- 917 [15] H. Grad. On the kinetic theory of rarefied gases. *Communications on Pure and*  
918 *Applied Mathematics*, 2(4):331–407, 1949.
- 919 [16] C. Groth and J. McDonald. Towards physically realizable and hyperbolic moment  
920 closures for kinetic theory. *Continuum Mech. Thermodyn.*, 21(467), 2009.
- 921 [17] J. Han, C. Ma, Z. Ma, and W. E. Uniformly accurate machine learning-based  
922 hydrodynamic models for kinetic equations. *Proceedings of the National Academy*  
923 *of Sciences*, 116(44):21983–21991, 2019.

- 924 [18] C. Hauck and R. McClarren. Positive PN closures. *SIAM Journal on Scientific*  
925 *Computing*, 32(5):2603–2626, 2010.
- 926 [19] M. Junk. Maximum entropy for reduced moment problems. *Mathematical Models*  
927 *and Methods in Applied Sciences*, 10(07):1001–1025, 2000.
- 928 [20] C. D. Levermore. Moment closure hierarchies for kinetic theories. *Journal of*  
929 *Statistical Physics*, 83(5):1021–1065, Jun 1996.
- 930 [21] L. R. Mead and N. Papanicolaou. Maximum entropy in the problem of moments.  
931 *Journal of Mathematical Physics*, 25(8):2404–2417, 1984.
- 932 [22] L. Mieussens. Discrete velocity model and implicit scheme for the BGK equation  
933 of rarefied gas dynamics. *Mathematical Models and Methods in Applied Sciences*,  
934 10(08):1121–1149, 2000.
- 935 [23] L. Mieussens. Convergence of a discrete-velocity model for the Boltzmann-BGK  
936 equation. *Computers & Mathematics with Applications*, 41(1):83 – 96, 2001.
- 937 [24] C. Ringhofer, C. Schmeiser, and A. Zwirchmayr. Moment methods for the semi-  
938 conductor Boltzmann equation on bounded position domains. *SIAM Journal on*  
939 *Numerical Analysis*, 39(3):1078–1095, 2001.
- 940 [25] M. Sadr, M. Torrilhon, and M. H. Gorji. Gaussian process regression for maxi-  
941 mum entropy distribution. *Journal of Computational Physics*, 418:109644, 2020.
- 942 [26] N. Sarna, J. Giesselmann, and M. Torrilhon. Convergence analysis of Grad’s  
943 Hermite expansion for linear kinetic equations. *SIAM Journal on Numerical*  
944 *Analysis*, 58(2):1164–1194, 2020.
- 945 [27] N. Sarna, H. Kapadia, and M. Torrilhon. Simultaneous-approximation-term  
946 based boundary discretization for moment equations of rarefied gas dynamics.  
947 *Journal of Computational Physics*, 407:109243, 2020.
- 948 [28] N. Sarna and M. Torrilhon. On stable wall boundary conditions for the Her-  
949 mite discretization of the linearised Boltzmann equation. *Journal of Statistical*  
950 *Physics*, 170(1):101–126, 2018.
- 951 [29] R. P. Schaerer, P. Bansal, and M. Torrilhon. Efficient algorithms and implemen-  
952 tations of entropy-based moment closures for rarefied gases. *Journal of Compu-*  
953 *tational Physics*, 340:138 – 159, 2017.
- 954 [30] R. P. Schaerer and M. Torrilhon. The 35-moment system with the maximum-  
955 entropy closure for rarefied gas flows. *European Journal of Mechanics - B/Fluids*,  
956 64:30 – 40, 2017.
- 957 [31] J. Schneider. Entropic approximation in kinetic theory. *ESAIM: M2AN*,  
958 38(3):541–561, 2004.
- 959 [32] H. Struchtrup. *Macroscopic Transport Equations for Rarefied Gas Flows*.  
960 Springer Ltd, 2010.
- 961 [33] E. Tadmor. Entropy stability theory for difference approximations of nonlin-  
962 ear conservation laws and related time-dependent problems. *Acta Numerica*,  
963 12:451–512, 2003.
- 964 [34] M. Torrilhon. Characteristic waves and dissipation in the 13-moment case. *Con-*  
965 *tinuum Mech. Thermodyn.*, 12:289–301, 2000.
- 966 [35] M. Torrilhon. Two-dimensional bulk microflow simulations based on regularized  
967 Grad’s 13-moment equations. *Multiscale Modeling & Simulation*, 5(3):695–728,  
968 2006.
- 969 [36] M. Torrilhon. Convergence study of moment approximations for boundary value  
970 problems of the Boltzmann-BGK equation. *Communications in Computational*  
971 *Physics*, 18(03):529–557, 2015.
- 972 [37] M. Torrilhon. Modeling nonequilibrium gas flow based on moment equations.  
973 *Annual Review of Fluid Mechanics*, 48(1):429–458, 2016.

- 974 [38] M. Torrilhon and N. Sarna. Hierarchical Boltzmann simulations and model error  
975 estimation. *Journal of Computational Physics*, 342:66 – 84, 2017.
- 976 [39] M. Torrilhon and H. Struchtrup. Regularized 13-moment equations: shock struc-  
977 ture calculations and comparison to Burnett models. *Journal of Fluid Mechanics*,  
978 513:171–198, 2004.
- 979 [40] S. Ukai. Solutions of the Boltzmann equation. In *Patterns and Waves*, volume 18  
980 of *Studies in Mathematics and Its Applications*, pages 37 – 96. Elsevier, 1986.
- 981 [41] J. Yang and J. Huang. Rarefied flow computations using nonlinear model Boltz-  
982 mann equations. *Journal of Computational Physics*, 120(2):323 – 339, 1995.
- 983 [42] Y. Ye and E. Tse. An extension of Karmarkar’s projective algorithm for convex  
984 quadratic programming. *Mathematical Programming*, 44:157–179, 1989.
- 985 [43] C. Zhenning, Y. Fan, and R. Li. Globally Hyperbolic Regularization of Grad’s  
986 Moment System. *Communications on Pure and Applied Mathematics*, 67(3):464–  
987 518, 2014.